


Research Article

New evidence from heavy minerals and detrital zircons in Quaternary fluvial sediments for the evolution of the upper Yangtze River, South China

Hengxu Huang^a, Fang Xiang^{a*} , Deyan Zhang^b, Yuming Guo^c, Qi Yang^c and Li Ding^c

^aInstitute of Sedimentary Geology, Chengdu University of Technology, Chengdu 610059, Sichuan, China; ^bInstitut für Geologie, Leibniz Universität Hannover, Hannover 30167, Germany and ^cCollege of Earth Sciences, Chengdu University of Technology, Chengdu 610059, Sichuan, China

Abstract

In the Three Gorges and adjacent areas, there are three planation surfaces and five terraces along the Yangtze River that record the evolution history of the river system. Here, we used diagnostic heavy minerals, U-Pb geochronology, and trace elements of detrital zircons from one planation surface, two terraces, and a modern point bar to reconstruct the evolution history of the upper Yangtze River, specifically the Chuan River in the Sichuan Basin. The sediments in the lowest planation surface had different felsic source rocks derived from east of the Three Gorges, which indicated that before the disintegration of the lowest planation surface (0.75 Ma), there were two paleorivers: the westward-flowing paleo-Chuan River and eastward-flowing paleo-Yangtze River separated by the Huangling Dome. At 0.75–0.73 Ma, the dominant detrital zircons from the Sichuan Basin in the sediments of terrace T₅ (the highest terrace) confirmed that the paleo-Yangtze River cut through the Three Gorges and captured the paleo-Chuan River, and the Daliang Mountains became the new drainage divide. Finally, the appearance of materials from the upper Jinsha River in terrace T₂ indicated that the paleo-Yangtze River progressively captured the paleo-Jinsha River, and the modern upper Yangtze River formed before 0.05 Ma. These river capture events of the upper Yangtze River confirmed the Quaternary uplift of the SE Tibetan Plateau.

Keywords: Heavy minerals, Zircon U-Pb chronology, Zircon trace element, Provenance analyses, Quaternary drainage evolution, Upper Yangtze River, Paleo-Chuan River, Three Gorges formation, Neotectonics, SE Tibetan Plateau

(Received 5 March 2022; accepted 4 October 2022)

INTRODUCTION

The formation and evolution of the Tibetan Plateau have profound implications for the understanding of continental deformation mechanics (Tapponnier et al., 2001). Most of the high-elevation landforms related to the plateau were distributed east of the main Himalayan collision zone, where the crustal volume increased more than 2×10^7 km³ in Cenozoic times (Clark et al., 2005). The crustal deformation and thickening in the southeastern Tibetan Plateau had a significant effect on large fluvial systems, landforms, and climate in East Asia (Brookfield, 1998; Zhong et al., 2018; McRivette et al., 2019; Li et al., 2020; Xiang et al., 2020; Li et al., 2022). Thus, research of river evolution can reveal the processes and degree of effect of the Tibetan Plateau tectonic activity on East Asia and its surrounding regions, and help us better understand the significance of the Tibetan Plateau uplift.

The Yangtze River originates in Tibet and flows through the southeastern Tibetan Plateau (Fig. 1), whose evolution mirrors the tectonic activity of the plateau and allows a reconstruction

of the surface uplift history of the plateau (Li, 1991; Pan et al., 2005a; Clift et al., 2006, 2008; Perrineau et al., 2011; Li et al., 2014). The Yangtze River can be divided into three segments based on tectonic and topographic units (Wang, 1985; Zhang et al., 2018): the Jinsha River from its headwaters to Yibin, the Chuan River from Yibin to Yichang (the Jinsha and Chuan Rivers together are called the upper Yangtze River), and the middle and lower reaches of the Yangtze River (Fig. 1c). In previous studies, more attention was paid to the Chuan River, especially in the Three Gorges area, because it holds a critical position, connecting the upper Yangtze River with the middle and lower Yangtze River (Yang et al., 2006; Liu et al., 2018; Sun et al., 2018). Tian et al. (1996) and Clark et al. (2004) proposed that there was a westward-flowing paleoriver west of the Three Gorges before the eastward-flowing Yangtze River appeared. Clift et al. (2006, 2008, 2020) conducted research on the Red River catchment in Vietnam and sedimentary rocks in SW China, and these works supported the presence of a paleoriver flowing from east to the west via the Three Gorges and Shigu (Fig. 1b) before the major reorganization of the ancient river systems. A paleoriver flowing westward from west of the Three Gorges was also proposed by Wang (2010) and Wang et al. (2013b, 2013c), based on an analysis of topographic gradients, logarithmic relationships of the drainage areas and distances, and confluence angles of the tributaries. Although the existence

*Corresponding author e-mail address: cdxiangfang@126.com

Cite this article: Huang H, Xiang F, Zhang D, Guo Y, Yang Q, Ding L (2023). New evidence from heavy minerals and detrital zircons in Quaternary fluvial sediments for the evolution of the upper Yangtze River, South China. *Quaternary Research* 113, 162–181. <https://doi.org/10.1017/qua.2022.58>

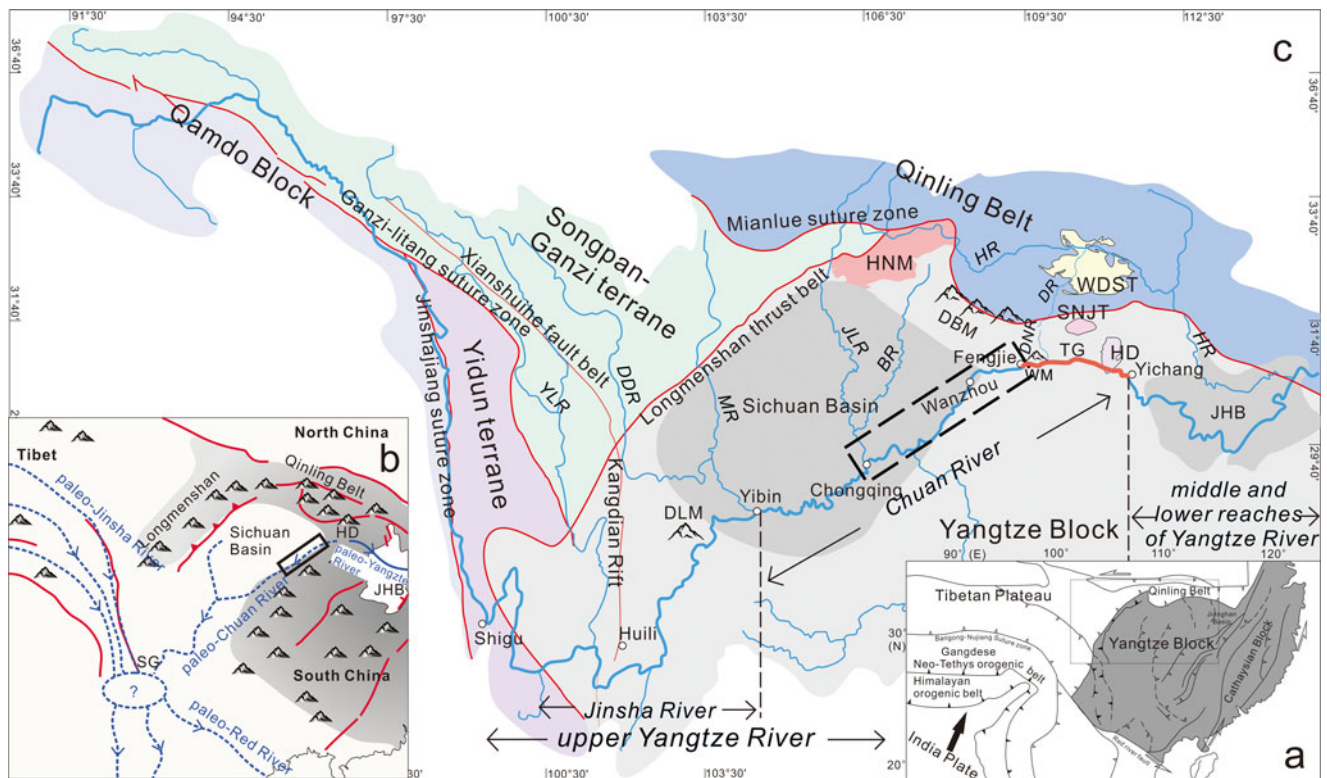


Figure 1. (a) Map showing the major tectonic blocks and the study area location. (b) Sketch map showing the tectonic-geomorphic framework before the birth of the modern Yangtze River. (c) Simplified tectonic map of the upper Yangtze River, adjacent orogenic belts and terranes; the dashed box indicates the study area (modified from Wang, 1985; Zheng, 2015). BR, Ba River; DBM, Daba Mountains; DDR, Dadu River; DLM, Daliang Mountains; DNR, Daning River; DR, Du River; HD, Huangling Dome; HNM, Hannan Massif; HR, Han River; JHB, Jiangnan Basin; JLR, Jialing River; MR, Min River; SG, Shigu; SNJT, Shennongjia terrane; TG, Three Gorges; WDSST, Wudangshan terrane; WM, Wu Mountain; YLR, Yalong River.

of the westward-flowing paleo-Chuan River before the Yangtze River reorganization was accepted by most geologists (Tian et al., 1996; Clark et al., 2004; Clift et al., 2006, 2008, 2020; Wang, 2010; Wang et al., 2013b, 2013c), little sedimentary evidence has been found to support this viewpoint.

Debate on the formation of the Three Gorges has continued. Most previous studies suggest that the formation age of the Three Gorges is 1.2–0.7 Ma (Pleistocene) based on studies of terraces in the Three Gorges, Quaternary deposits in the Jiangnan Basin, and continuous cores of boreholes in the Yangtze delta (Tang and Tao, 1997; Li et al., 2001; Yang et al., 2006; Wang et al., 2009; Xiang et al., 2011, 2018; Liu et al., 2018; Sun et al., 2018). Other studies, however, have indicated that the Three Gorges formed before the Pliocene, based on the fluvial deposition in the lower reaches of the Yangtze River, detrital zircons in the Yangtze delta, Nd and Pb isotopes in the sediments of the Hanoi Basin, and the Cenozoic sediments in the Jiangnan Basin and offshore basins in East China (Clift et al., 2008; Jia et al., 2010; Zheng et al., 2013; Yang et al., 2019; Fu et al., 2021; Sun et al., 2021; Zhang et al., 2021). Despite disagreement surrounding the formation time of the Three Gorges, previous studies have indicated that the opening of the Three Gorges was an important capture event that led to the birth of the modern Yangtze River (Yang et al., 2006; Wang et al., 2009; Jia et al., 2010; Liu et al., 2018; Sun et al., 2018).

The formation of Three Gorges was a crucial Yangtze River drainage reorganization event. However, the entire upper Yangtze River, which extends 4504 km from the headwaters to

the Three Gorges (Liu et al., 2020b), could not possibly have formed at the same time as the opening of the Three Gorges. Thus, a coherent drainage evolution pattern of the upper Yangtze River is required to describe the reorganization process of the entire upper Yangtze River.

Step-like landforms, such as planation surfaces and terraces, are well preserved in the Three Gorges region. Sediments in these landforms recorded how source areas changed through time, which also reflects the evolution history of the upper Yangtze River. Thus, we studied the heavy mineral compositions and the ages and trace element chemistry of detrital zircons collected from the lowest planation surface, two river terraces, and a modern point bar in the study area that extends from Chongqing to Fengjie to establish a chronology of source area change to acquire evidence of the westward-flowing paleo-Chuan River, constrain the formation timing of the Three Gorges, and clarify the evolution process of the Chuan River.

GEOLOGIC BACKGROUND

The study includes the area from Chongqing to Fengjie along the upper Yangtze River, from 31°3′24.5″N, 109°32′51.8″E to 29°30′37.5″N, 106°31′14.3″E. The study area is lower in the west and higher in the east, and the Sichuan and Jiangnan Basins form the western and eastern boundaries, respectively. The Han River, one of the major tributaries of the Yangtze River, flows along the northern margin of the study area and empties into the Yangtze River in Wuhan city. Three planation surfaces

(planation surface: a remnant surface caused by regionally different uplift after the end of planation) and five terraces can be identified in the study area. The highest planation surface is the E'xi planation surface, with elevations between 1700 and 2000 m above sea level (m asl), which cuts mainly across limestone and was the drainage divide between the main stream and major tributaries of the Yangtze River in the Three Gorges area (Shen, 1965). The second-highest planation surface, the Shanyuan planation surface, is composed of valley and intermountain basins and uvala that are inlaid in the E'xi planation surface, with altitudes ranging from 800 to 1200 m asl. Both the E'xi and Shanyuan planation surfaces are generally believed to have formed before the Quaternary (Shen, 1965; Tian *et al.*, 1996). The lowest planation surface, the Yunmeng planation surface, with an elevation of approximately 600 m asl, is considered to have formed from fluvial processes during the Early Pleistocene (Tian *et al.*, 1996; Li *et al.*, 2001).

There are five main terraces (e.g., T₅–T₁, in descending order from oldest to youngest) below the Yunmeng planation surface along the slopes of the Yangtze River Gorges. Terraces T₅ and T₄ are mainly pedestal terraces, whereas terraces T₁–T₃ are accumulation terraces (Tian *et al.*, 1996; Xiang, 2004; Xiang *et al.*, 2005). The detailed sedimentary characteristics of the terrace outcrops are discussed in the next section.

Rocks with provenance significance in the upper Yangtze River catchment are shown in Figure 2. Distinctive age distributions of exposed bedrock in four lithotectonic rock groups allow detrital zircon ages to be linked to source areas. Rock group I is distributed in the Huangling Dome and Shennongjia terrane, which are

exposed in the area of the drainage divide between the paleo-Yangtze River and paleo-Chuan River (Wang, 1985; Zhang *et al.*, 2018). In the Huangling Dome, highly metamorphosed Archean basement is the oldest rock exposed in the Yangtze Block and has yielded igneous crystallization and metamorphic zircon growth ages, apparently of 2947–2913 Ma (Qiu *et al.*, 2000; Wei *et al.*, 2009; Wei and Wang, 2012; Zhao *et al.*, 2012). The Neoproterozoic Huangling granitoids yielded zircons with U–Pb ages of 837 Ma in the Huangling Dome (Gao and Zhang, 2009; Zhang *et al.*, 2009).

Rock group II is distributed in the South Qinling Belt and Wudangshan terrane, which are separated from the Yangtze Block by the Mianlue suture zone and belong to the Han River catchment (Fig. 2). Neoproterozoic granite with ages of 943–689 Ma (Ma, 2002), island arc igneous rock with ages of 295–264 Ma (Lai and Qin, 2010), and Indosinian collisional granite with ages of 220–189 Ma (Hu *et al.*, 2004; Yang *et al.*, 2009; Meng *et al.*, 2013; Fang *et al.*, 2017) are exposed in the South Qinling Belt. Additionally, Paleoproterozoic gneiss outcrops in the South Qinling Belt have yielded zircons with U–Pb ages of 2284–1853 Ma (Ma, 2002; Zhang *et al.*, 2002). The Neoproterozoic igneous rock in the Wudangshan terrane yielded ages that are tightly clustered at 755 Ma (Ling *et al.*, 2010).

Rock group III is distributed in the Sichuan Basin and Hannan Massif to the west of the Three Gorges and is exposed in the Chuan River catchment (Fig. 2). An abundance of Mesozoic clastic sediments is exposed in the Sichuan Basin, among which the Middle Jurassic red continental clastic rocks, the Shaximiao Formation,

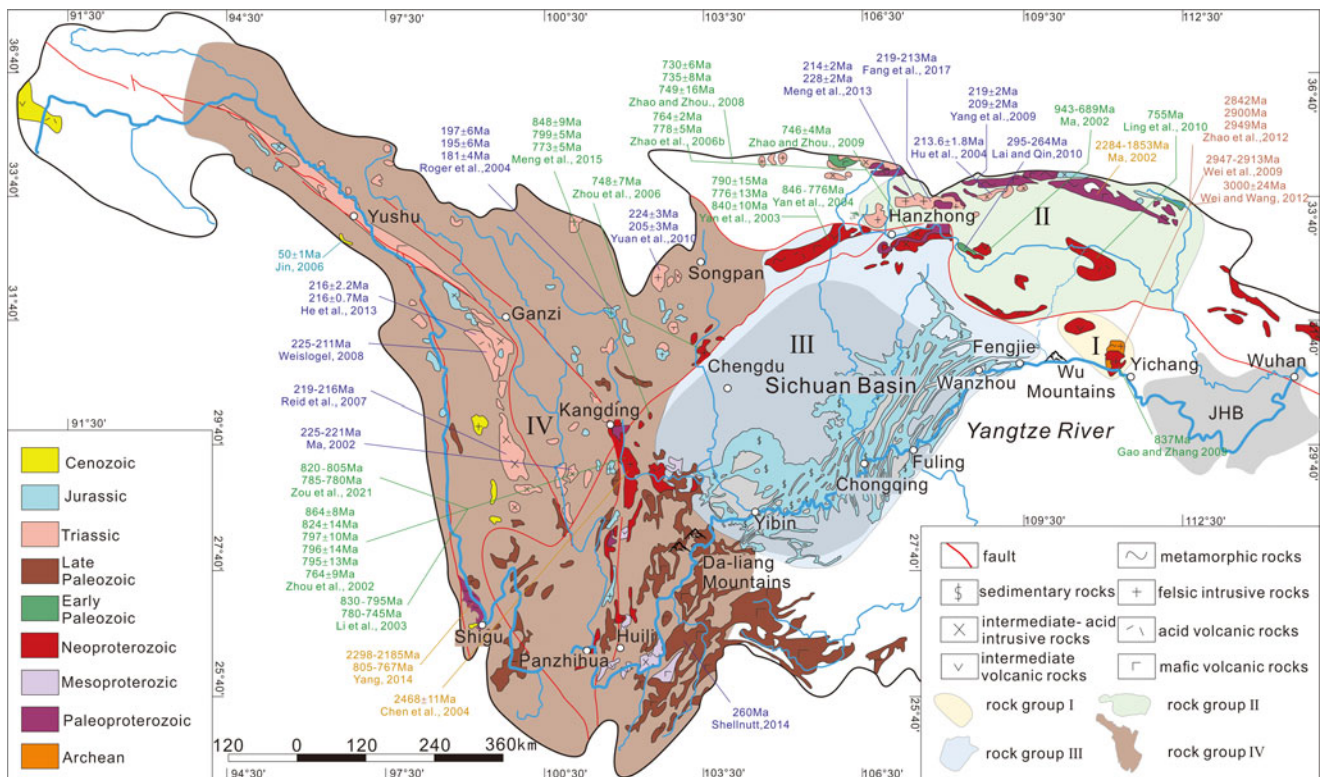


Figure 2. Sketch showing the zircon U–Pb ages and distribution of igneous rocks and metamorphic rocks in the upper Yangtze River (after Jia *et al.*, 2010; Wang and Fan, 2013; Huang *et al.*, 2016; Li *et al.*, 2018). I, Huangling Dome and Shennongjia terrane; II, South Qinling Belt and Wudangshan terrane; III, Sichuan Basin and adjacent region; IV, Qamdo Block, Yidun terrane, Songpan–Ganzi terrane, and Kangdian Rift. Ma, 2002; Zhou *et al.*, 2002, 2006; Li *et al.*, 2003; Yan *et al.*, 2003, 2004; Chen *et al.*, 2004; Hu *et al.*, 2004; Roger *et al.*, 2004; Jin, 2006; Zhao *et al.*, 2006b, 2012; Reid *et al.*, 2007; Weislogel, 2008; Zhao and Zhou, 2008, 2009; Gao and Zhang, 2009; Wei *et al.*, 2009; Yang *et al.*, 2009; Lai and Qin, 2010; Ling *et al.*, 2010; Yuan *et al.*, 2010; Wei and Wang, 2012; He *et al.*, 2013; Meng *et al.*, 2013, 2015; Shellnutt, 2014; Yang, 2014; Fang *et al.*, 2017; Zou *et al.*, 2021.

are widely distributed in the southern part of the Sichuan Basin. The Shaximiao Formation contains grayish-purple fine-grained quartz sandstone, arkosic sandstone, purple-red siltstone, and mudstone and reaches more than 2000 m in maximum thickness (BGMRSF, 1991). Paleoproterozoic intermediate-felsic rocks and mafic rocks are widespread in the Hannan Massif and are dated between 780 Ma and 689 Ma (Yan et al., 2003, 2004; Zhao et al., 2006b; Zhao and Zhou, 2008, 2009; Wang et al., 2012).

Rock group IV is distributed in the Qamdo Block, Yidun terrane, Songpan-Ganzi terrane, and Kangdian Rift and is exposed in the Jinsha River catchment (Fig. 2). Cenozoic intermediate to felsic igneous rocks crop out in the Qamdo Block (55–40 Ma; Jin, 2006). The Yidun terrane consists of a flysch-volcanic succession, the Triassic Yidun Group (BGMRSF, 1991), and arc-related granitoid plutons with predominant ages of 225–202 Ma (Reid et al., 2007; Weislogel, 2008; He et al., 2013). The detrital zircon ages of the Yidun Group are characterized by major age populations of 240–220 Ma, 480–400 Ma, 1000–720 Ma, 1900–1700 Ma, and 2500–2400 Ma (Wang et al., 2013a). The Paleoproterozoic metamorphic units of the Shigu Group, which are located along the Jinshajiang suture zone, are a medium- to low-grade metamorphic series and yield zircon crystallization ages of 805–767 Ma and 2298–2185 Ma (Yang, 2014). The Songpan-Ganzi terrane is characterized by a 5- to 10-km-thick Late Triassic flysch (Zhou and Graham, 1996) and by the intrusion of Mesozoic granitoids with ages of 195–153 Ma and 225–205 Ma (Roger et al., 2004; Yuan et al., 2010). Neoproterozoic mafic to felsic igneous rocks are widely exposed in the Kangdian Rift, with ages of 860–750 Ma (Zhou et al., 2002; Li et al., 2003; Zhang, 2020; Zou et al., 2021). Triassic granitoids are exposed in the Kangdian Rift, with ages of 225–221 Ma (Ma, 2002). Paleoproterozoic metamorphic complexes, which are known as the basement of the Yangtze Block, are exposed in the Kangdian Rift, with an oldest age of 2468 Ma (Chen et al., 2004). In addition, Neoproterozoic intermediate and felsic plutonic rocks are exposed in the Longmenshan thrust belt and are dated to between 859 Ma and 699 Ma (Ma et al., 1996; Zhou et al., 2006; Meng et al., 2015). The late Permian Emeishan Large igneous province (ELIP) on the western margin of the Yangtze Block yielded ages tightly clustered at 260 Ma (Li, 2012; Shellnutt, 2014; Huang et al., 2016).

OUTCROP SEDIMENTARY CHARACTERISTICS AND SAMPLE LOCATIONS

The outcrop of the Yunmeng planation surface is located in the Fengjie area (31°03′24.5″N, 109°32′51.8″E, 554 ± 7 m asl). Located below an overlying slide-related gravel layer, the fluvial deposits have the following characteristics: (1) the lower segment consists of 8- to 15-cm-thick yellow-brown sandy clay, from which sample PT01 was collected (Fig. 3). (2) The middle segment consists of 1- to 3-cm-thick gray clay. (3) The upper segment consists of a 30- to 80-cm-thick gravel layer that is intercalated with brownish-red sandy clay, in which are found subspherical 1.5- to 4-cm-long pebbles composed of flint, siliceous limestone, quartz sandstone, and other components and having a preferred orientation. Sample PT02 was collected from sandy interstitial materials (Fig. 3). The electron spin resonance (ESR) age of the quartz grains from the sand interstitial material in the upper gravel layer is 0.75 Ma, which is comparable with the planation surface age of 0.8–0.75 Ma in the Yichang area (ESR age from Xiang et al. [2005]).

Terrace T₅ of the Yangtze River is represented by an outcrop (29°30′37.5″N, 106°31′14.3″E, 286 ± 12 m asl) in the Chongqing

area, which consists of a gravel layer mixed with brownish-yellow sand that is in unconformable contact with the bedrock under a fluvial swash surface. The compositions of the clasts in the ca. 10-m-thick gravel layers are quartzite and quartz sandstone along with some severely weathered granite, basalt, andesite, and porphyry. The gravels form an imbricated structure with the maximum flat surface trending to the southwest (210°–230°) (Fig. 3). The ESR age of the gravel layer is between 0.73 and 0.7 Ma (Xiang et al., 2005, 2020). Sample TTL01 was collected from brownish-yellow interstitial sand materials (Fig. 3).

Terrace T₂ of the Yangtze River is represented by an outcrop (31°49′53.9″N, 108°26′54.7″E, 160 ± 7 m asl) in the Wanzhou area and is an accumulation terrace composed of a 15-m-thick khaki-colored sandy clay layer with caliche nodules. Sample WTL01 was collected from the lower part of the outcrop (Fig. 3). The results of the previous ¹⁴C dating of calcareous nodules and ESR dating (Tian et al., 1996; Li et al., 2001) showed that the age of terrace T₂ is between 0.05 and 0.03 Ma.

Sample W was taken from the sandy sediments in a modern point bar in the Wanzhou area (30°49′53.9″N, 108°26′54.7″E). Because suitable sampling outcrops of terraces T₄, T₃, and T₁ were not found in our fieldwork, we constrained the earliest capture event of the upper Yangtze River using the provenance information of lowest planation surface and terrace T₅, and constrained the formation age of the modern upper Yangtze River using terrace T₂ and the modern point bar. Information about the sample locations is given in Supplementary Table S1.

ANALYTICAL METHODS

The transparent heavy minerals (see Table 1) were disaggregated and separated from sediments by standard heavy liquid methods, using the 4–2 φ (63–250 μm) size fraction (Thompson, 1974; Garzanti et al., 2009). For each sample, 200 points were counted in grain mounts at suitable regular spacing under the petrographic microscope to determine the relative abundance of heavy minerals (Galehouse, 1971; Mange and Maurer, 1992). The ZTR, T&, LgM and HgM indices were calculated to quantitatively express the heavy mineral concentration in each sample. The ZTR index, reflecting the chemical durability of sedimentary rock, is the sum of volume percentages of zircon, tourmaline, and rutile over total transparent heavy minerals (Hubert, 1962). The T& index is the volume percentage of relatively stable heavy minerals in total transparent heavy minerals, including the titanium-containing minerals sphene, anatase, and brookite, as well as monazite, xenotime, apatite, and barite. LgM and HgM indices (LgM, including epidote, clinozoisite, zoisite, allanite, piemontite, prehnite, pumpellyite, carpholite, lawsonite chloritoid; HgM, including staurolite, andalusite, kyanite, and sillimanite) can be used to judge low- and high-grade metamorphic source rocks (Garzanti and Andò, 2007a, 2007b).

To avoid overlooking particles present in small amounts, all types of zircons were selected and separated from each sample by hand-picking under a binocular microscope according to their color, size, degree of roundness, and crystal morphology; cracked crystals were excluded. The systematic classification scheme of zircon morphology from Piper et al. (2012) was adopted in the sample analysis process.

High-spatial-resolution U-Th-Pb data and trace element composition were analyzed on the same target spots of each zircon at the State Key Laboratory of Geological Processes and Mineral Resources, China University of Geosciences, using an Agilent HP7500a inductively coupled plasma-mass spectrometer equipped

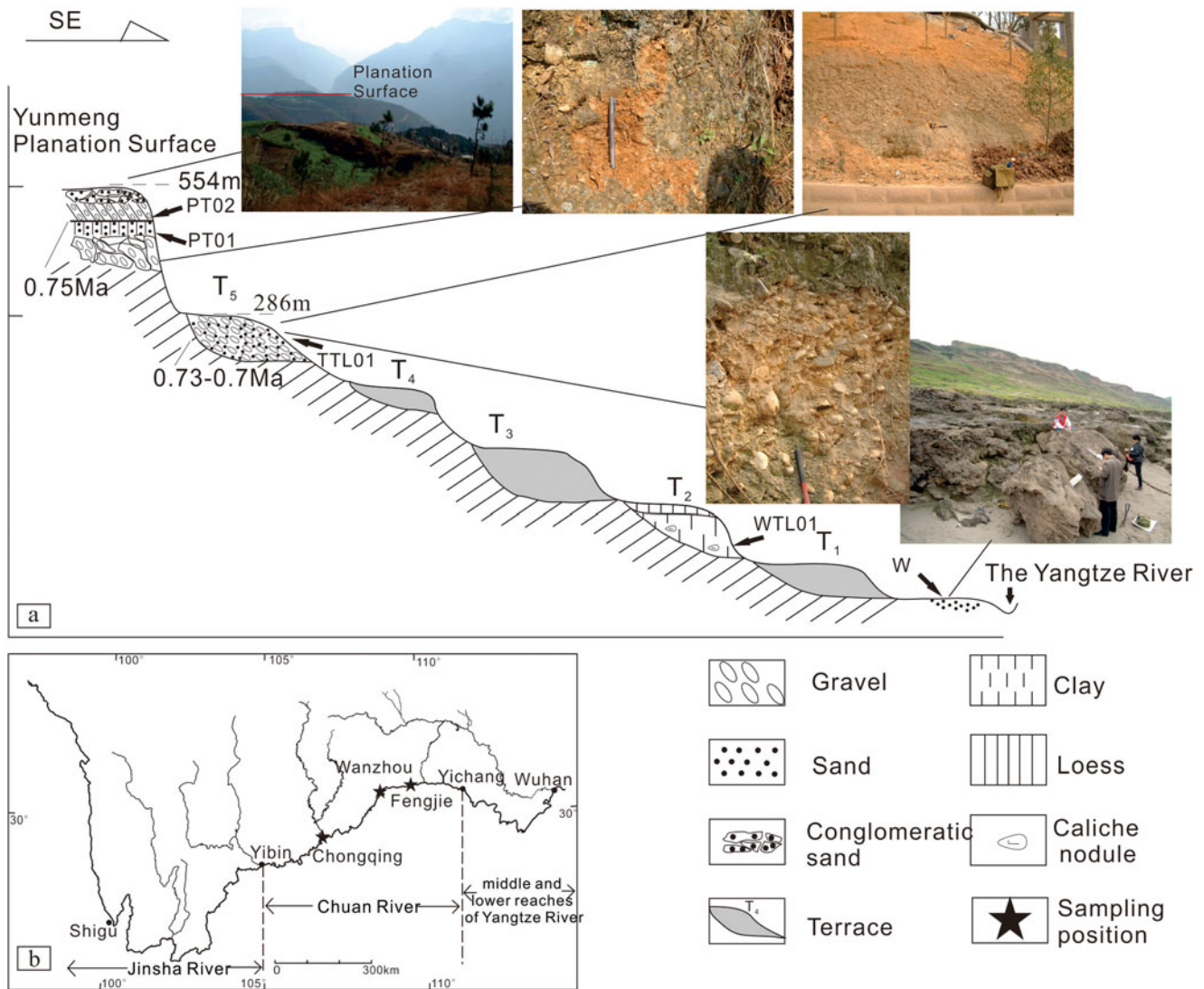


Figure 3. Sampling location and profile. (a) Composite profile of fluvial sediments and sampling points. (b) Sampling location. Insets show distant prospective and profiles of the Yunmeng planation surface and terraces.

with a 213 nm laser ablation device (Geo Las 2005). Helium was used as the carrier for the ablation material. The experimental data were processed using ICPMS Data Cal software (Liu *et al.*, 2008, 2010) with GJ and 91500 as external standards by applying Anderson's normal lead correction procedure (Andersen, 2002), and were filtered using a $\pm 10\%$ discordance cutoff. The $^{206}\text{Pb}/^{238}\text{U}$ ratio was used for grains with ages younger than 1000 Ma, and the $^{207}\text{Pb}/^{206}\text{Pb}$ ratio was used for grains older than 1000 Ma (Sircombe, 1999; Cawood and Nemchin, 2000). The kernel density estimate (KDE) plots and multidimensional scaling (MDS) plots were obtained using Provenance, a software package within the R statistical programming environment (Vermeesch, 2012; Vermeesch *et al.*, 2016).

RESULTS

Type and content of heavy minerals

The detailed statistics on heavy minerals from every sample are shown in Table 1 and Figure 4. Notably, apatite and pyroxene exist in each sample. Because these minerals are the most prone to

chemical weathering in superficial deposits (Bateman and Catt, 1985, 2007), their appearance indicates that sediments on the Yunmeng planation surface and terraces have not suffered severe sub-aerial weathering, so the initial provenance information of heavy minerals that are more resistant than apatite and pyroxene is trustworthy.

Every sample contains zircon, rutile, and tourmaline, which are the most strongly resistant to both mechanical and chemical weathering. However, the amount of epidote, amphibole, garnet, titanite, anatase, and pyroxene varies in each sample. The content of apatite in samples PT02, WTL01, and W is more than that in sample TTL01, but it is zero in sample PT01. Additionally, some minerals only appear in a certain sample: monazite only appears in sample PT01, allanite only appears in sample PT02, barite only appears in sample TTL01, tremolite only appears in sample WTL01, and kyanite only appears in sample W.

ZTR and T& indices are higher than 20 in samples PT01 and PT02, but are lower than 10 in samples TTL01, WTL01, and W. The LgM index indicates that detritus from low-grade metamorphic source rocks is absent in samples PT01 and PT02, but abundant in samples TTL01, WTL01, and W. The HgM index

Table 1. Statistics of transparent heavy mineral content in samples and their potential source rocks.

	Sample ^a Mineral species ^b	PT01	PT02	TTL01	WTL01	W	Potential source rocks of heavy minerals ^c
Volume of percentage of detrital heavy minerals (%)	Zircon	9.64	15.20	3.88	2.79	2.31	Rocks of crustal origin, particularly ubiquitous in silicic and intermediate igneous rocks
	Rutile	4.82	5.57	1.12	1.9	1.65	Metamorphic rocks, particularly in schists, gneisses, amphibolites
	Tourmaline	6.49	7.50	3.40	1.44	Exist	Granites, granite pegmatites, pneumatolitic veins, and contact or regional metamorphite
	Epidote	Exist	Exist	87.12	32.85	46.21	Greenschist-facies regional metamorphite, contact metamorphic rocks, and dynamic metamorphic basic igneous rocks
	Pyroxene	Exist	8.93	Exist	43.53	27.52	Various ultramafic, basic to intermediate igneous rocks, particularly gabbros, dolerites, andesites, basalts, and some peridotites
	Apatite		1.22	Exist	0.77	2.04	Almost all types of igneous rocks
	Amphibole			Exist	6.98	10.90	Igneous rock: intermediate, acid, and alkaline intrusive igneous rocks; metamorphic rocks: greenschist facies, amphibolite facies, and granulite facies
	Garnet	Exist		Exist	2.2	4.30	Variety of metamorphic rocks and plutonic igneous rock, pegmatites, ultramafic, and some acid volcanics
	Titanite		Exist	2.71	4.23	2.13	Undersaturated and intermediate plutonic rocks; metamorphic schists, granite-gneisses, amphibolites, and metamorphosed impure calc-silicate rocks
	Anatase	64.79	28.19	0.49	1.9	0.60	Igneous and metamorphic rocks
	Leucosene	14.26	33.38	1.19	1.23	2.22	Authigenic mineral
	Monazite	Exist					Granitic rocks, rarely in metamorphic schist, gneisses, and granulites
	Allanite		Exist				Granite, granodiorite, and syenite, partially in pegmatites, schists, and gneisses
	Barite			0.11			Metalliferous hydrothermal veins or as cementing medium in sandstones
	Tremolite				0.19		Thermal or regional metamorphism of siliceous dolomites
	Kyanite					0.13	Gneisses, granulites, and pelitic schists
Indices	ZTR	20.95	28.28	8.40	6.12	3.96	
	T&	64.79	29.42	3.30	6.90	4.77	
	LgM			87.12	32.85	46.21	
	HgM					0.13	

^a“Exist” indicates the mineral was found by accident in a quantity too small to weigh.

^bZTR = total volume percentage of ultrastable minerals (zircon, tourmaline, and rutile); T& = total volume percentage of titanium minerals (sphene, anatase, and brookite) and others (e.g., apatite, monazite, and barite); LgM = total volume percentage of low-grade metamorphic minerals (e.g., epidote group, chloritoid, carpholite, and lawsonite); HgM = total volume percentage of high-metamorphic minerals (staurolite, andalusite, kyanite, and sillimanite).

^cPotential provenance refers to: Marmo, 1971; Force, 1980; Mange and Maurer, 1992; Ma et al., 2019.

reveals that some high-grade metamorphic rocks exposed in the Yangtze River catchment may have become the source rock for sample W.

In addition, sample WTL01 bears much resemblance to sample W in both heavy mineral species and contents, which implies lack of significant differences of source materials between these two samples. In other words, the river system underwent little change during the depositional period of terrace T₂ and modern

point bar; thus, sample WTL01, collected from terrace T₂, was not selected for further analysis.

Morphology, zoning, and Th/U ratio of detrital zircons

To describe the difference of each zircon assemblage in each sample, the zircon morphology and zoning classification scheme was adopted (Triantafyllidis et al., 2008; Piper et al., 2012). Based on

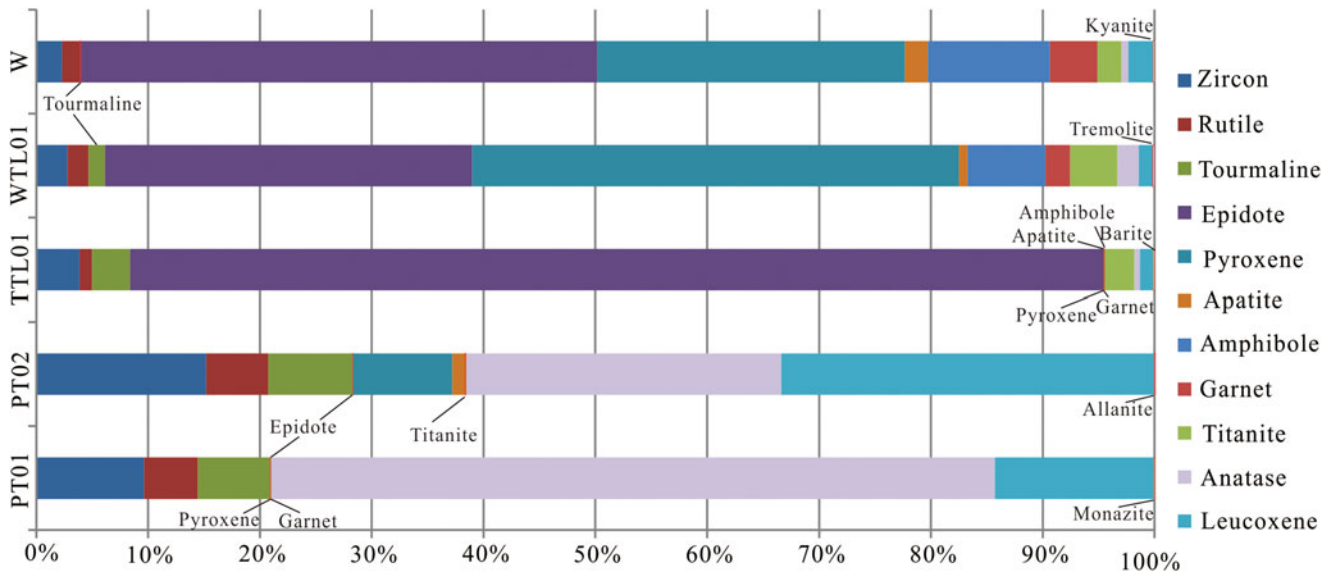


Figure 4. Heavy mineral abundances of all samples plotted as volume percentages.

the sample classification scheme, type 1 zircons represent igneous first-cycle zircons, which have sharp edges and planar faces and generally contain inclusions and faces with resorption. Type 2 is identified as metamorphic zircon grains, which are ordinarily rounded to subrounded and anhedral, lack regular, parallel oscillatory zoning, and display some resorbed, pitted, or subhedral features. Type 3 contains recycled grains, which are rounded or irregular and pitted, with igneous zoning crosscut by the broken or abraded grain edge. Type 1 zircons could also be divided into five subgroups: type 1A, with complete oscillatory zoning; type 1B, with an internal corrosion surface; type 1C, containing

inclusions and with zoning; type 1D, lacking inclusions but with zoning and resorbed faces; and type 1G, having almost no visible zoning but with euhedral to subhedral crystals (Piper *et al.*, 2012).

The cathode luminescence (CL) images and morphologic variability in different zircon types of the four samples were systematically researched (Fig. 5). From the Yunneng planation surface to terrace T₅ and modern point bar, the abundance of types 1A, 1C, and 1D of igneous zircon is stable, but the abundance of metamorphic zircons progressively decreases. Sample PT01 from the lower segment of the Yunneng planation surface has more

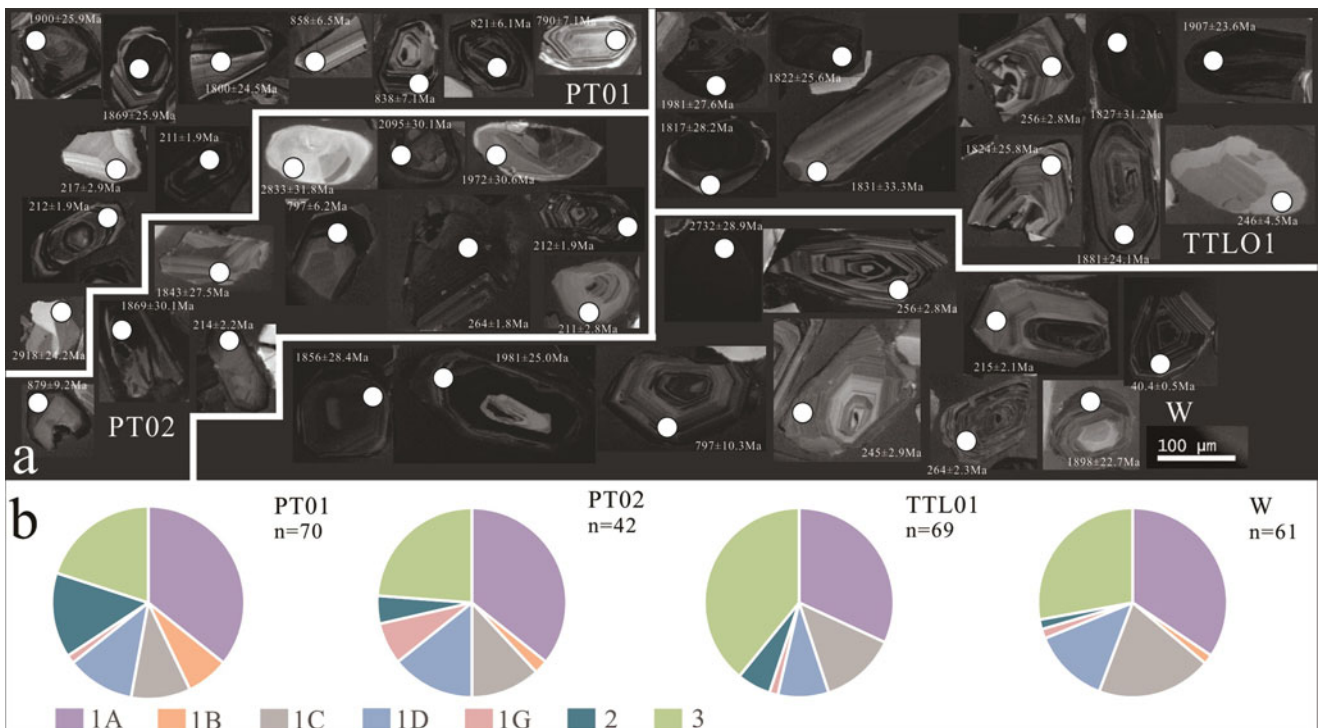


Figure 5. Cathodoluminescence images (a) and relative abundance (b) of different zoning types in zircon grains from the four samples. n = number of grains.

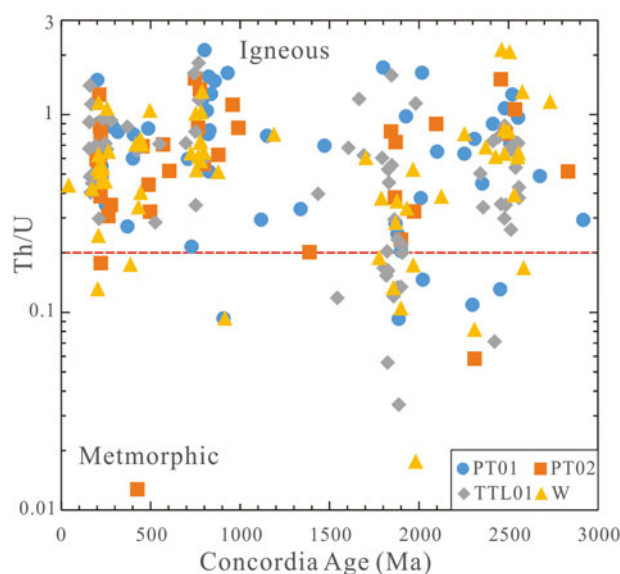


Figure 6. Th/U ratios plotted against concordant U-Pb ages for all analyzed detrital zircon grains from the four samples.

metamorphic grains than sample PT02 from the upper segment. The zircon type in terrace T₅ in the Fengjie area is different from that in other samples. The zircon assemblage is dominated by the igneous type 1A and type 3: 32% of type 1A and 39% of type 3.

Th/U ratio as a source indicator was taken into consideration when estimating provenance of detrital zircons (Maas et al., 1992). Combined with CL images, the Th/U values can be used to reflect parent rock characteristics and distinguish igneous from metamorphic zircons (Schulz et al., 2006; Harley et al., 2007). According to the Th/U values, zircons derived from igneous rocks account for more than 87.6% of whole zircon grains in all samples analyzed (Fig. 6). Among these, igneous zircons account for 91.4% in sample PT01, 92.9% in sample PT02, 84.1% in sample TTL01, and 83.6% in sample W.

U-Pb age of detrital zircons

Taking into consideration the variability of large fluvial systems such as the Yangtze River, the KDE (Fig. 7) and MDS (Fig. 8a) plots are used to show the range of zircon ages in this study by comparing them with zircon U-Pb ages of channel sand from the main stream and major tributaries in the Sichuan and Jiangnan Basins, as well as the Mesozoic clastic rocks in the Sichuan Basin (He et al., 2014; Li et al., 2018). The data with the greatest relevance would be closest within the MDS plot. Specific ages and concordant diagrams of all zircon grains analyzed in this work can be found in Supplementary Table S2 and Supplementary Figure S1.

The zircon age spectra of samples PT01 and PT02, collected from the Yunmeng planation surface, show certain similarity with channel sand from the main stream of the Yangtze River in Yichang and the Han River, in that the abundance of the Mesozoic (300–100 Ma) and Neoproterozoic (1000–600 Ma) zircon grains is greater than those of the Paleo-Mesoproterozoic (2100–1500 Ma) and Paleoproterozoic (2600–2200 Ma; Figs. 7 and 8a). The sediments from the Yunmeng planation surface also contain several Archean zircon grains (older than 2600 Ma).

The zircon populations of sample TTL01, collected from terrace T₅, show a significant similarity with that of the Jialing

River (Fig. 8a) with respect to the abundance of Mesozoic, Neoproterozoic, Paleo-Mesoproterozoic, and Paleoproterozoic zircon grains.

Sample W shows a multisource with a number of distinctive zircon populations, such as Paleozoic zircon grains (600–300 Ma) and a single Paleogene grain (40 Ma), similar to main stream channel sand of the Yangtze River in the Fuling area (Figs. 7 and 8a).

Trace element character of detrital zircons

The contents of trace elements of detrital zircons from four samples are shown in Supplementary Table S3. The geochemical composition of zircons shows an overall decrease in U, Gd, and Ce content from samples PT-01 and PT-02 (62.3–2155.3, 3–322, and 1–173 ppm, respectively) to samples TTL01 and W (34–1505, 2–96, and 0–83 ppm, respectively). Their Yb contents range from 6 to 1554 ppm in four samples.

DISCUSSION

Implications of zircon geochemistry

The geochemistry of zircons is a sensitive indicator of their parental magma compositions and accessory minerals. Thus, the identification of accessory minerals by elemental information from a single crystal offers a powerful approach to determine the provenance (Grimes et al., 2015).

The zircon's affinity for U, Yb, and other heavy earth elements (HREEs) permits these elements to be incorporated into zircon crystals so that the U/Yb ratio of zircon will reflect that of the parental melt when it crystallized. Differences in the U/Yb ratio value can be used to discriminate between ocean crust zircon and continental zircon (Grimes et al., 2007). A U/Yb ratio <0.1 is generally characteristic of zircons from the normal mid-ocean ridge basalt and other similar mantle sources. Continental arc zircon has U/Yb mostly between 0.1 and 4, and Grimes et al. (2015) attributed this higher value to greater influence from mature, large-ion lithophile-enriched crust during formation of the parental melts. Meanwhile, accessory minerals have an obvious effect on the trace elemental ratios in zircon (Kirkland et al., 2015), so this influence should be taken into consideration when fingerprinting a zircon source.

When crystallized, a previously formed zircon has a lower U/Yb ratio than a later-formed zircon. The relatively high concentration of HREE in titanite and apatite also results in increased U/Yb in the melt (Grimes et al., 2015), and element fractionation in zircon with apatite will increase Nb/Yb of the melt with increasing U/Yb, and these influence for melt would be recorded in later-formed zircons. Crystallization of titanite or ilmenite will decrease Nb/Yb but increase U/Yb of zircon (Grimes et al., 2015; Figs. 9 and 10). Higher Gd/Yb is a good proxy for enrichment of middle REE relative to heavy REE, and a higher value is an indicator of garnet growth with or before growth of magmatic or metamorphic zircon (Grimes et al., 2015). A higher Ce/Yb ratio of zircon reflects the enrichment of light REE relative to heavy REE. Because titanite (with apatite) and monazite preferentially incorporate light and middle rare earth elements from the melt, rather than heavy rare earth elements, their presence will result in a decrease in Gd/Yb and Ce/Yb ratios in co-crystallizing zircon. Compared with the Gd/Yb and Ce/Yb ratios in most of the mid-ocean ridge suite, the decrease in Gd/Yb ratio and increase

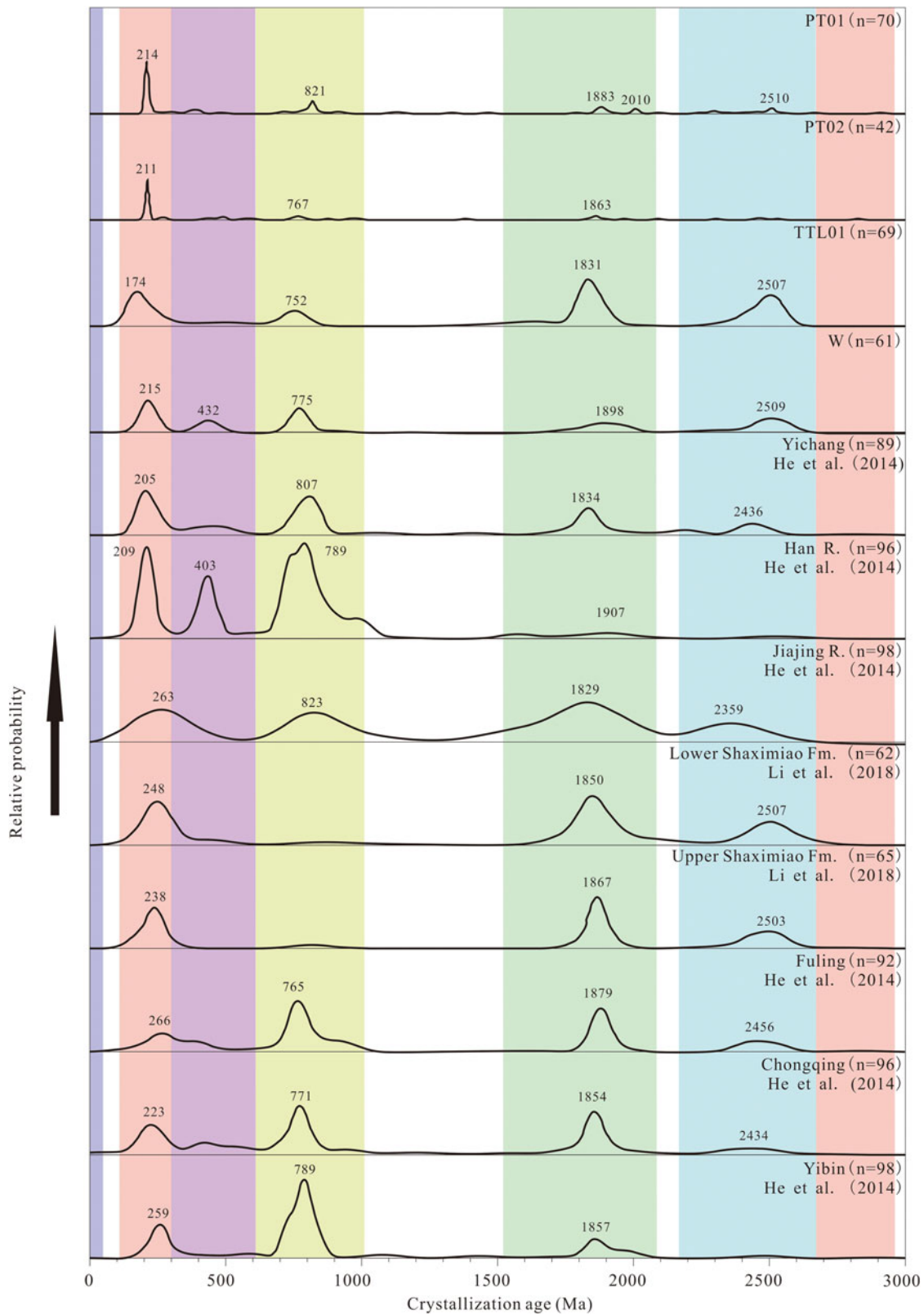


Figure 7. Kernel density estimate (KDE) plots of the detrital zircon U-Pb ages. n = total amount of zircons in each sample. He et al., 2014; Li et al., 2018.

in Ce/Yb ratio of zircon can be ascribed to the influence of melt cooling and zircon crystallization (Bea, 1996; Grimes et al., 2015; Figs. 9 and 10).

All zircon grains analyzed show high U/Yb ratios (>0.1) and are determined to be from continental settings (Grimes et al., 2007, 2015). The Archean zircon populations in samples PT01

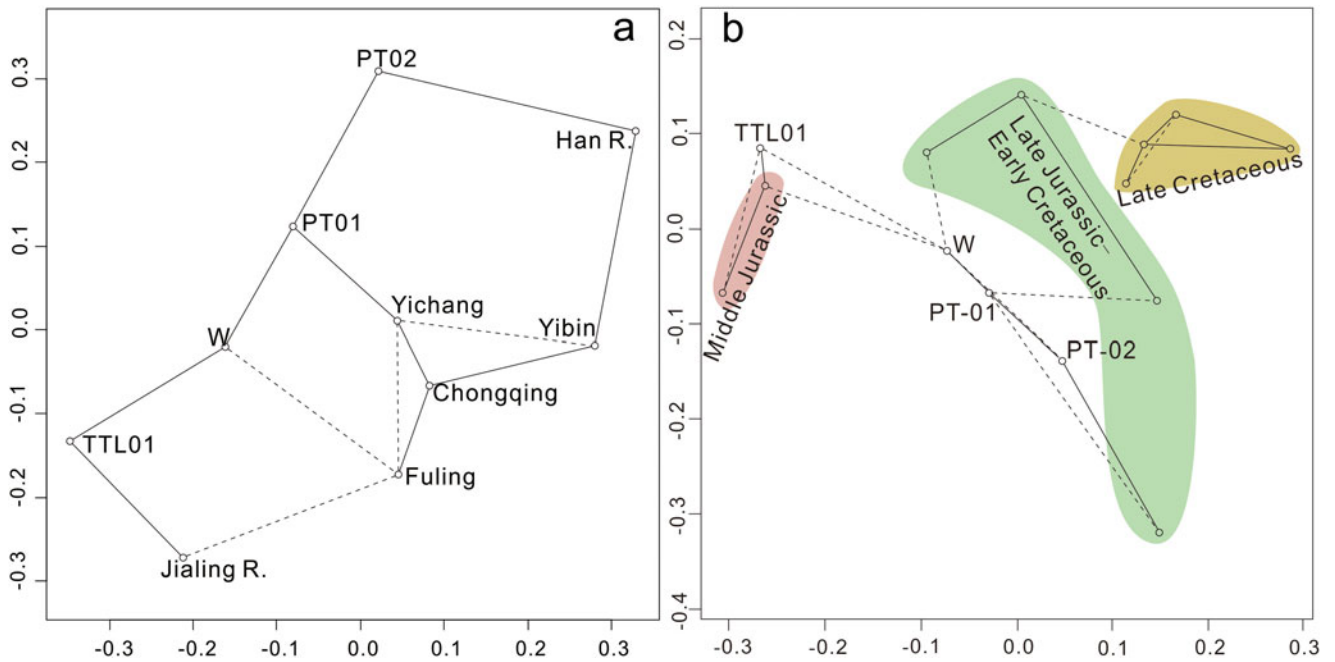


Figure 8. Multidimensional scaling (MDS) plot of the four samples' detrital zircon data as well as the Middle Jurassic to Late Cretaceous detrital zircon data, generated using methods outlined by Vermeesch et al. (2016). Solid and dashed lines mark the nearest and the second nearest neighbors, respectively. Age data of the Mesozoic clastic rocks in southern Sichuan Basin are from Li et al. (2018); strata with different ages are highlighted by different colors.

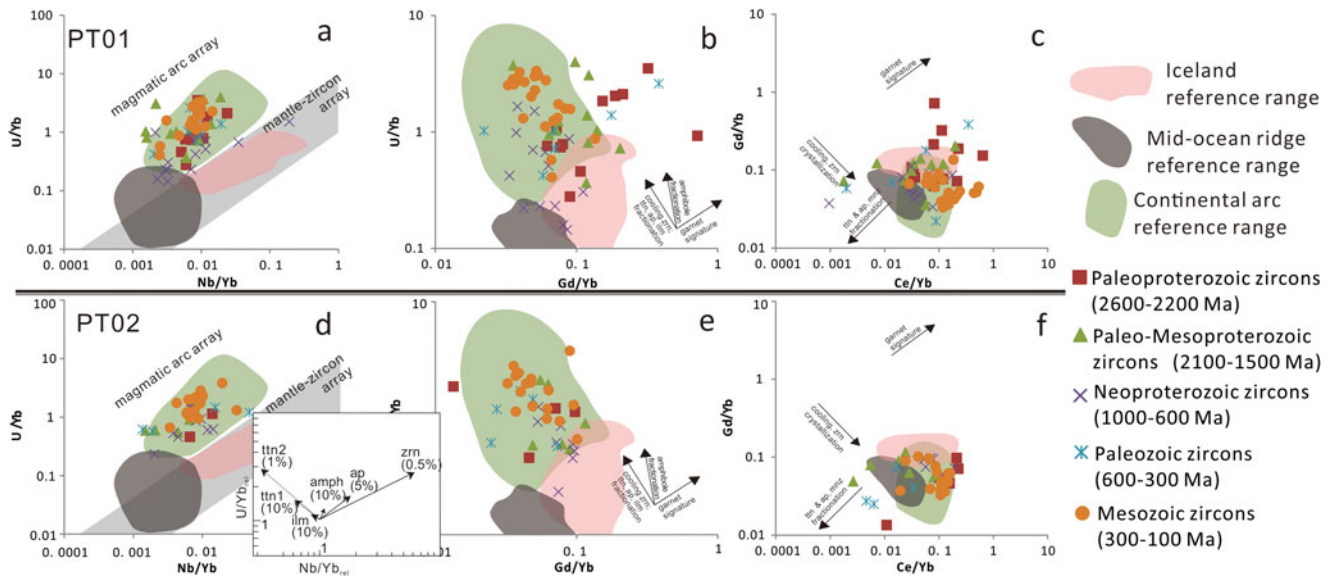


Figure 9. Petrogenetic interpretation diagram of zircons in samples PT01 and PT02. Mid-ocean ridge basalt data are from Lehnert et al. (2000). Iceland lava composition is from Carley et al. (2011, 2014). The continental arc lava data are from Carley et al. (2014). The upper boundaries in a and d are placed at the Nb/Yb (0.004, 0.02) and U/Yb endpoints (1, 10). The inset in d shows the effect of open-system (Rayleigh) fractionation of select minerals on U/Yb and Nb/Yb ratios of the remaining melt (and later-formed zircons) relative to initial ratios = 1. Vectors are shown to scale for the extent of fractional removal (of that mineral only) indicated by the percentages listed. The distribution coefficients used are from Grimes et al. (2015). amph, amphibole; ap, apatite; ilm, ilmenite; mnz, monazite; ttn, titanite; zrn, zircon.

and PT02 and Paleogene grains in sample W have only single grains without a fractionation trend and are not included here. On the Yunmeng planation surface (samples PT01 and PT02), the Paleoproterozoic zircon population has relatively increasing and decreasing Gd/Yb ratios along with increasing U/Yb ratio and is inferred to have formed with accessory garnet and titanite. The Paleo-Mesoproterozoic zircon grains have relatively

low Gd/Yb and Ce/Yb ratios and exhibit the characteristics of co-crystallization with titanite (with apatite). The Neoproterozoic and Mesozoic populations have increasing Nb/Yb ratios along with increasing U/Yb ratios relative to the continental arc reference range, resulting in the trajectory shown in Figure 9a, which would be approximately parallel to the mantle-zircon array, implying the enrichment of zircons. The Paleozoic

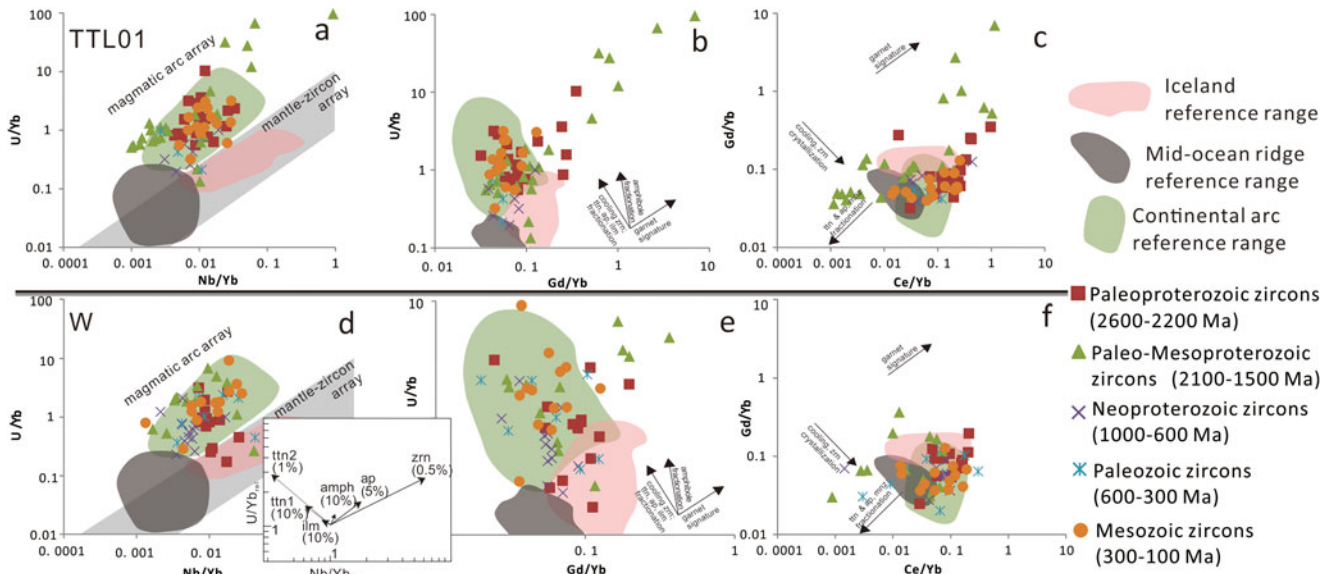


Figure 10. Petrogenetic interpretation diagram of zircons in samples TTL01 and W. amph, amphibole; ap, apatite; ilm, ilmenite; mnz, monazite; ttn, titanite; zrn, zircon.

zircon grains have increasing and decreasing Ce/Yb ratios along with decreasing Gd/Yb ratios, as shown in Figure 9c and f, which indicates the influence of titanite, monazite, and zircon crystallization.

In sample TTL01, which was collected from terrace T₅, the Paleoproterozoic zircons show two trajectories of increasing Gd/Yb ratios along with the U/Yb ratios and constant Gd/Yb ratios with increasing U/Yb ratios, as shown in Figure 10b, which indicate garnet-abundant and amphibole-abundant fractionation trends, respectively. The Paleo-Mesoproterozoic zircon grains show two trajectories that are subparallel and orthogonal to the mantle-zircon array, as shown in Figure 10a, and indicate two fractionation trends of garnet and titanite (with apatite), as shown in Figure 10b and c. The Neoproterozoic zircons are skewed at a high angle to the mantle-zircon array, as shown in Figure 10a, and exhibit constant Gd/Yb ratios and increasing U/Yb ratios, as shown in Figure 10b, which indicate the fractionation trend of accessory amphibole. The Paleozoic zircon grains have a trajectory that is orthogonal to the mantle-zircon array, as shown in Figure 10a, and decreasing Gd/Yb ratios with increasing U/Yb ratios, as shown in Figure 10b, while the Mesozoic zircon grains exhibit decreasing Gd/Yb ratios along with decreasing Ce/Yb ratios, as shown in Figure 10c, all of which show the influence of titanite co-crystallization.

In sample W, which was collected from the modern point bar, the Paleoproterozoic, Neoproterozoic, and Paleozoic zircon populations are orthogonal and skewed with low angles to the mantle-zircon array, as shown in Figure 10d, and show two fractionation trends in which the Gd/Yb ratios remain stable and decrease with increasing U/Yb ratios, as shown in Figure 10e, which indicate the presence of titanite, apatite, and amphibolite during the crystallization process. The Paleo-Mesoproterozoic zircons show two trends in which the Gd/Yb ratios decrease or increase with increasing U/Yb ratios (Fig. 10e), which implies the influence of titanite, apatite, and garnet crystallization. The Mesozoic zircons are subparallel to the mantle-zircon array, as shown in Figure 10d, and exhibit a trend for which the U/Yb and Ce/Yb

ratios increase with decreasing Gd/Yb ratios, as shown in Figure 10e and f, which could be influenced by prior zircon crystallization.

In general, the zircon populations on the Yunmeng planation surface exhibit the geochemical characteristics of co-crystallizing with felsic igneous minerals such as zircon and monazite, whereas the zircons in the terrace and modern point bar crystallized with mafic igneous minerals, such as amphibole. This distinction can also be found in the provenances indicated by heavy mineral composition.

Provenance evidence from heavy minerals and detrital zircons in sediments

Provenance of sediments on the Yunmeng planation surface

The relatively high ZTR and T& indices in samples PT01 and PT02 indicate chemical durability. The Archean, Paleoproterozoic, and Paleo-Mesoproterozoic zircon populations from the Yunmeng planation surface show rounded to subrounded morphologies with absent or indistinct oscillatory zoning under CL, belonging mainly to type 2 zircons. The zircon trace element characteristics indicate the Archean, Paleoproterozoic, and Paleo-Mesoproterozoic zircon populations co-crystallized with titanite and garnet. In fact, Archean rock in the Yangtze River catchment is exposed only in the Huangling Dome of rock group I (Wang and Fan, 2013; Fig. 2), which underwent multistage magmatic (3000–2900 Ma, 2700–2600 Ma, and 1870–1850 Ma) and metamorphic events (2600–2500 Ma and 2050–1900 Ma). The Archean rock yielded abundant titanites, garnets and zircons with type 2 morphology (Zhao *et al.*, 2006a; Wei *et al.*, 2020). Thus, the Archean, Paleoproterozoic, and Paleo-Mesoproterozoic zircon populations from the Yunmeng planation surface can only be derived from rock group I. Meanwhile, this also indicates the existence of a paleo-river flowing from the Huangling Dome to the Fengjie area that deposited sediments on the Yunmeng planation surface.

The Neoproterozoic zircon grains are observed to have prismatic and short prismatic shapes with complete oscillatory zoning

and inclusions, with features of types 1A and 1C. The trace elements of the Neoproterozoic zircon group show characteristics of co-crystallization of zircon and monazite, indicating these zircons were derived from felsic rock. The Huangling granitoids in rock group I were intruded into the Huangling Dome in the Neoproterozoic. The Huangling granitoids yielded abundant tremolites, monazites, and zircons, among which zircon grains show short prismatic shapes with oscillatory zoning and a peak age of 837 Ma and partial zircon grains contained inclusions (Ma, 2002; Gao and Zhang, 2009). Thus, the Huangling granitoids in rock group I are most likely source rocks of tremolites, monazites, and the Neoproterozoic zircon grains.

Mesozoic zircons with the trace element characteristics of felsic igneous zircons display complete oscillatory zoning and long and prismatic shapes, belonging mainly to type 1A. However, few Triassic rocks are exposed around the study area, except for rock group II to the north of the study area (Fig. 2). The Triassic granites in rock group II yielded plenty of zircons with an age range of 219–213 Ma and type 1A, 1C, and 1D morphologies (Hu et al., 2004; Yang et al., 2009; Meng et al., 2013; Fang et al., 2017). Thus, we believe that the high density of Mesozoic zircons is likely the input result of rock group II to the north of the study area, which is also supported by the similarity of sediments from the Yunmeng planation surface to the channel sand of the Han River (Fig. 8a).

Provenance of sediments in terrace T₅

The heavy mineral assemblage in sample TTL01 is dominated by epidotes with a high LgM index and contains a few barites and garnets. The Paleoproterozoic and Paleo-Mesoproterozoic zircon populations are dominated by recycled grains with type 3 morphology (rounded or irregular shapes, broken or abraded grain edge, and weak and dark oscillatory zoning). All of these features indicate the provenance characteristics of clastic sediments in the tectonic setting of an “undissected Craton subprovenance” (Garzanti and Andò, 2007b). Considering the similarity of the zircon age spectra of terrace T₅ and the Jialing River (Fig. 7) and the large volumes of Mesozoic clastic rocks in the Sichuan Basin of rock group III, we assessed the contribution of Mesozoic clastic rocks in the Sichuan Basin to the sediments in terrace T₅. The detrital zircon age data from all samples and the available published Middle Jurassic to Late Cretaceous sediments plot in the MDS plot (Vermeesch et al., 2016; Fig. 8b).

Sample TTL01 shows significant affinity with the Middle Jurassic Shaximiao Formation of rock group III located in the southern Sichuan Basin as a potential sediment source (Figs. 2 and 8b), but without affinity to Late Jurassic or Cretaceous sedimentary rocks. Despite the affinity of the zircon age distributions between sample TTL01 and the Middle Jurassic Shaximiao Formation, the lack of a Neoproterozoic zircon population in the Shaximiao Formation and the difference in peak age values of the Mesozoic zircon population in sample TTL01 (174 Ma), the Shaximiao Formation (248 and 238 Ma; Li et al., 2018), and the Jialing River channel sand (263 Ma; He et al., 2014) suggest the existence of additional Neoproterozoic and Mesozoic sources for the sediments of terrace T₅. Numerous felsic-intermediate and mafic intrusions occur in the Hannan Massif of rock group III. These intrusions yield abundant amphiboles and zircons, from which zircons with crystallization ages of 780–689 Ma are euhedral and oscillatory zoned, tallying with type 1A morphology (Zhao et al., 2006b; Zhao and Zhou, 2008, 2009). The Neoproterozoic zircons (789–696 Ma) in sample TTL01 are

euhedral prismatic shapes with complete oscillatory zoning, and some grains have inclusions, belonging mainly to type 1A and 1C morphologies. Zircon trace elements instruct that these zircons crystallized concurrently with amphibole. Thus, amphiboles and the Neoproterozoic zircons appear to be derived from the Hannan Massif of rock group III.

The Mesozoic zircon population with a peak age of 174 Ma has long and short prismatic shapes with complete oscillatory zoning, belonging to the morphologic features of types 1A and 1C. These zircons show the zircon trace element characteristic of co-crystallization with titanite. Many granitic plutons in the Songpan-Ganzi terrane of rock group IV were considered to be Mesozoic intrusions, which yielded abundant zircon, titanite, and apatite (Roger et al., 2004; Fig. 2). These zircons yielded from granitic plutons show long prismatic and columnar shapes and complete but relatively dark oscillatory zoning with a peak age of 181 Ma and are influenced by co-crystallization with titanite (Roger et al., 2004; Wu et al., 2021). Thus, titanite, apatite, and the Mesozoic zircons in sample TTL01 were likely transported from granitic plutons in the Songpan-Ganzi terrane of rock group IV by drainage in the western Sichuan Basin, such as the Min River.

Provenance of sediments in the modern point bar

Considering that Cenozoic rocks are exposed only in the Qamdo Block of rock group IV in the Yangtze River catchment (Fig. 2), the only Paleogene zircon from the modern point bar was surely derived from there. The Mesozoic zircons with a peak age of 215 Ma, are fine, long, and prismatic and have complete oscillatory zoning; grains belonging to types 1A, 1C, and 1D have inclusions and resorbed faces. The Mesozoic zircons are identified as felsic igneous zircons according to the trace element characteristics (Fig. 10d). The granitoid plutons of the Yidun terrane of rock group IV yielded a number of zircons with an age range of 245–216 Ma and type 1A and 1D morphologies (Reid et al., 2007; Fig. 2). The Mesozoic zircons were likely derived from the granitoid plutons of the Yidun terrane.

The Paleozoic zircon population shows complete oscillatory zoning, and some granules have inclusions and rounded shapes with morphologic features of types 1A, 1C, and 3. However, early Paleozoic strata are exposed in the Qinling orogeny and the Cathaysia Block (Dong et al., 2011, 2013; Wang and Fan, 2013; Zhang et al., 2013), and it was not possible for these to be deposited in the study area. The Yidun Group of the Yidun terrane in rock group IV with a detrital age population of 480–400 Ma was most likely the source of these Paleozoic zircons (Wang et al., 2013a).

The Neoproterozoic zircons have oscillatory zoning. The majority of these grains have inclusions and partly irregular shapes, suggesting type 1C, 1A, and 3 morphologies, with a peak age of 775 Ma; trace elements indicate their co-crystallization with titanite, apatite, and amphibole. The Shigu Group yielded abundant titanites and zircons, with zircons having broken prismatic shapes with oscillatory zoning and a weighting average age of 805±18 Ma (Yang, 2014). The Neoproterozoic rocks of the Longmenshan thrust belt contain plenty of amphibole and apatite. Zircons in these Neoproterozoic rocks have short prismatic shapes with complete oscillatory zoning and have age peaks at 740 Ma, 748 Ma, and 770 Ma (Ma et al., 1996; Zhou et al., 2006; Meng et al., 2015; Zou et al., 2020). The Neoproterozoic granites in the Kangdian Rift yielded abundant zircons with an age range of 773–721 Ma, short prismatic shapes, and oscillatory zoning with

Table 2. Potential sources of every age group in four samples.

Sample ^a Age group	PT01	PT02	TTL01		W
40–50 Ma	—	—	—		Rock group IV: Qamdo Block
100–300 Ma	Rock group II: South Qinling Belt		Rock group IV: Southern Songpan-Ganzi terrane		Rock group IV: Yidun terrane
300–600 Ma	—	—	—		Rock group IV: Yidun terrane
600–1000 Ma	Rock group I: Huangling Dome; rock group II: Wudangshan terrane	Rock group II: Wudangshan terrane	Rock group III: Hannan Massif	Rock group III: Sichuan Basin	Rock group IV: Longmenshan thrust belt and Kangdian Rift
1500–2100 Ma			—		Rock group IV: Kangdian Rift and Yidun terrane
2200–2600 Ma	Rock group I: Huangling Dome		—		Rock group IV: Shigu Group, Yidun terrane, and Kangdian Rift
Older than 2600 Ma			—		—

^aA dash (—) indicates that there is no source information for this age group in samples.

inclusions (Zhou et al., 2002; Chen et al., 2004). Thus, titanite, apatite, amphibole, and Neoproterozoic zircons in sample W were possibly derived from these Neoproterozoic rocks in rock group IV.

The Paleo-Mesoproterozoic zircons show co-crystallization characteristic with titanite, apatite, and garnet under the instruction of zircon trace elements and have complete oscillatory zoning and equiaxed, short prismatic, or partially rounded-subrounded shapes similar to the morphologic features of types 1A and 3. There is garnet-mica schist in the southern Huili area, which yielded zircons with ages of 2026–1825 Ma, and garnet grains, among which zircons are short prismatic and oscillatory zoned with partially resorbed faces (Guan et al., 2011). In addition, the Yidun Group is also characterized by detrital zircon ages of 1900–1700 Ma (Wang et al., 2013a). These titanite, apatite, garnet, and Paleo-Mesoproterozoic zircon grains were likely derived from schist in Huili area and rocks in the Yidun Group.

The Paleoproterozoic zircons show short prismatic, broken, irregular shapes with oscillatory zoning, and some grains have inclusions belonging to type 1A, 1C, and 3 morphologies. The trace element characteristic of the Paleoproterozoic zircon population indicates influence of co-crystallization with titanite, apatite, and amphibole. However, the oldest zircons on the western margin of the Yangtze Block consist of the metamorphic zircons of the Shigu Group (2298–2185 Ma; Yang, 2014), detrital zircons of the Yidun Group (2500–2400 Ma; Wang et al., 2013a) and zircons in the Paleoproterozoic rocks of the Kangdian Rift in rock group IV (Ma, 2002). Therefore, titanite, apatite, amphibole, and the Paleoproterozoic zircon grains were possibly derived from these rocks.

In addition, the heavy mineral composition of sample W contains abundant pyroxene and amphibole and is associated with the widespread late Permian ELIP of rock group IV. However, the mantle sources of the ELIP yield low-zircon abundances, which result in the lack of correlative zircon records in sample W (Li, 2012; Shellnutt, 2014).

The potential sources of all zircon samples are shown in Table 2.

Evolution of the upper Yangtze River

Wang (1985) and Zhang et al. (2018) proposed that the paleo-Yangtze River system consisted of three segments before they were connected into one large river. The first segment, the paleo-Jinsha River, extended from the headwaters to Shigu and flowed southward (Fig. 11). The second segment, the paleo-Chuan River, flowed westward from the Huangling Dome to Shigu and then turned southward to the paleo-Red River (Clift et al., 2006, 2008; Zheng, 2015; Gourbet et al., 2017; Fig. 1b). The third segment, called the paleo-Yangtze River, extended from the Huangling Dome to the East China Sea and flowed eastward.

Among the sediments, the clast compositions of the gravel layer on the Yunmeng planation surface consist mainly of quartzite, flint, siliceous limestone, and sandstone, but those in terrace T₅ consist of basalt, andesite, and porphyry. Combined with the characteristics of the heavy mineral assemblages and zircon trace elements, the sediments on the surface of the Yunmeng planation are derived from felsic rocks of rock groups I and II (Fig. 2). However, the sediments in terrace T₅ are derived from the sedimentary and mafic rocks of rock groups III and IV (Fig. 2). The pronounced distinction between the source rocks of the Yunmeng planation surface and those of terrace T₅ supports the occurrence of a large-scale drainage reversal in the Three Gorges area when the Yunmeng planation surface disintegrated and sediments began to be deposited on terrace T₅. The ESR ages of the sediments on the Yunmeng planation surface and terrace T₅ are ca. 0.75 Ma and 0.73–0.7 Ma, respectively (Xiang et al., 2005, 2020), so we believe that the paleo-Chuan River flowed westward before 0.75 Ma and reversed to flow eastward between 0.75 Ma and 0.73 Ma (Fig. 11a and b). At the same time, the reversal time of the paleo-Chuan River should coincide with the opening time of the Three Gorges, and this reversal process is thought to be the result of the paleo-Chuan River being captured by the paleo-Yangtze River (Tian et al., 1996; Clark et al., 2004).

The potential eastern provenance of the Yunmeng planation surface is the Huangling Dome, which implies that the drainage

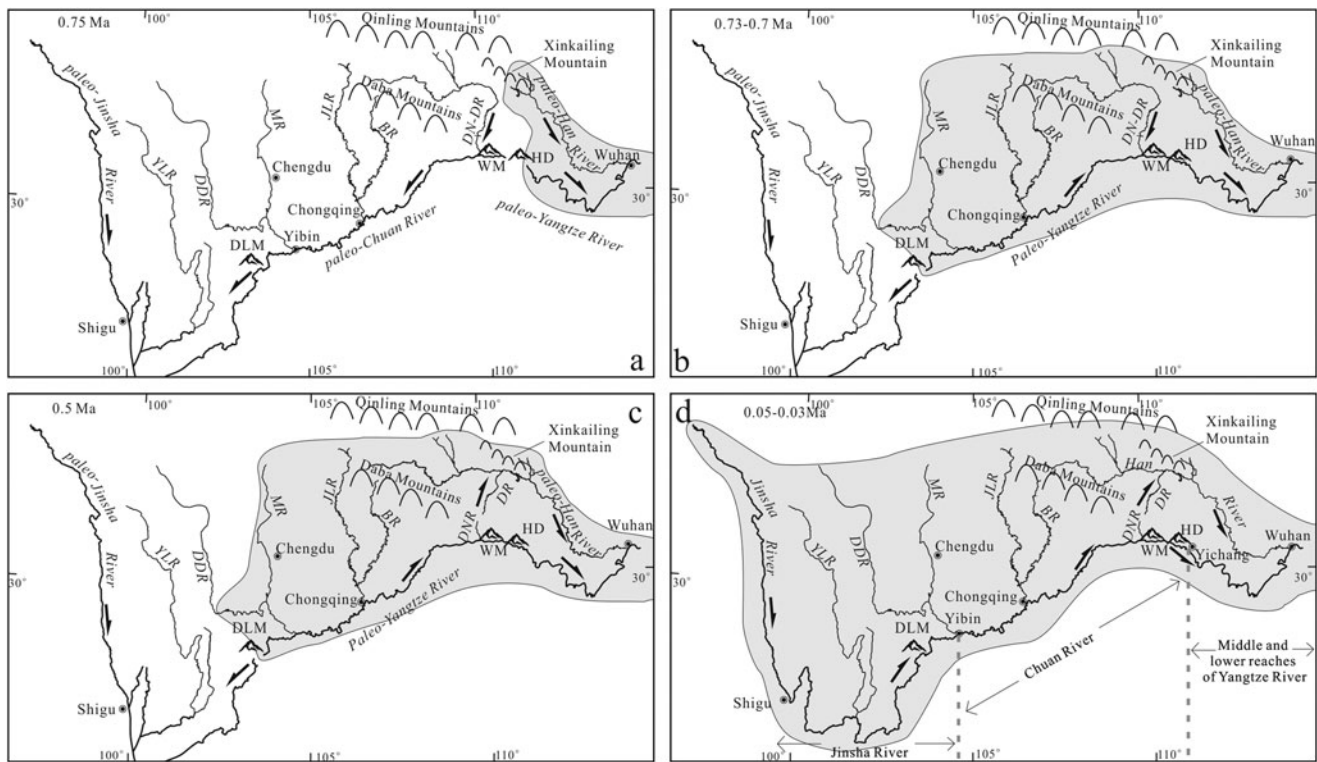


Figure 11. The evolution model for the upper Yangtze River. (a) The Huangling Dome was the drainage divide between the paleo-Yangtze River and the paleo-Chuan River at 0.75 Ma. (b) The paleo-Yangtze River captured the paleo-Chuan River, and the drainage divide retreated to the Daliang Mountains at 0.73–0.7 Ma. (c) The Daning–Du River was divided into two rivers, and the modern Han River formed at 0.5 Ma. (d) The modern Yangtze River formed before 0.05 Ma. BR, Ba River; DDR, Dadu River; DLM, Daliang Mountains; DN-DR, Daning–Du River; HD, Huangling Dome; JLR, Jialing River; MR, Min River; WM, Wu Mountain; YLR, Yalong River.

divide between the paleo-Chuan River and paleo-Yangtze River was located in the Huangling Dome at that time (Fig. 11a). There are abundant clasts from rock group II on the Yunmeng planation surface that could not have been deposited in the Fengjie area by the paleo-Han River with a modern drainage shape. An ancient river channel in the Huangling Dome area should have existed to connect the South Qinling Belt area with the Fengjie area when these clasts were being deposited (i.e., 0.75 Ma). In the eastern Daba Mountains area, the valleys of the Daning and Du Rivers, as tributaries of the Yangtze River and Han River, respectively, are now separated by a drainage divide in the Daba Mountains area that is located to the west of the Huangling Dome (Fig. 11d). It is possible that the Daning and Du Rivers are remnants of the paleoriver channel that connected the South Qinling Belt and Fengjie area. The paleoriver channel divided into the Daning River and Du River as a result of Cenozoic tectonic activity and episodic uplift that started at 0.5 Ma in the Daba Mountains area (Fu et al., 2014; Zhang et al., 2014; Fig. 11b and c).

The sediments in terrace T₅ are mainly derived from rock group III, which indicates that the paleo-Yangtze River captured the Jialing River. Most of sediments in terrace T₅ are from the Shaximiao Formation in the Sichuan Basin of rock group III, the proportion of which is even higher than in the modern point bar. This is possibly because the formation of the Three Gorges would lower the base level of erosion in the Sichuan Basin and further intensify regional denudation and would also simultaneously provide an outlet for erosional detritus (Richardson et al., 2010). Thus, the erosional detritus that is

widely distributed in the southern Sichuan Basin was deposited near the Yangtze River valley in the Chongqing area when sediments were deposited in terrace T₅. Meanwhile, the scarcity of mafic igneous minerals such as pyroxene indicates that the detritus from the main body of the ELIP of rock group IV was not carried into the paleo-Yangtze River catchment at that time. These rocks are widespread in the western Yibin region (Fig. 2). Thus, the drainage divide between the paleo-Yangtze River and paleo-Chuan River would migrate to the Daliang Mountains in western Yibin (Fig. 11b). The sediments in the modern point bar are derived from the Shigu Group, Yidun terrane, Kangdian Rift, and Qamdo Block of rock group IV and indicate the formation of the modern Yangtze River. Despite the lack of zircon age data in terrace T₂ in the Wanzhou area, the heavy mineral assemblage of sample WTL01 is similar to that in the modern point bar, with abundant mafic igneous minerals such as amphiboles and pyroxenes, especially tremolites from the Shigu Group of rock group IV. Therefore, the modern Yangtze River should date back to a time before sediments were deposited in terrace T₂ (0.05–0.03 Ma; Fig. 11d).

Accordingly, we propose the following evolution model for the Chuan River: at 0.75 Ma, the drainage divide between the paleo-Yangtze River and paleo-Chuan River was located in the Huangling Dome. At 0.75–0.73 Ma, the Three Gorges was cut through, the paleo-Chuan River was captured by the paleo-Yangtze River, and the drainage had migrated to the Daliang Mountains. At 0.7–0.05 Ma, the paleo-Yangtze River captured the paleo-Jinsha River, and a uniform large river system—the Yangtze River—formed.

Cenozoic regional uplift and the evolution of the upper Yangtze River

Fluvial incision can be a response to tectonic activity, climate change, and sea-level fluctuation (Hartshorn *et al.*, 2002; Pratt *et al.*, 2002; Dortch *et al.*, 2011b). However, due to the long distance from the study area to shore, the influence of sea level might be negligible. On long-term (10^4 – 10^5 years) timescales, fluvial incision rates always maintain consistency with rates of surface uplift in a tectonically active region (Hartshorn *et al.*, 2002; Dortch *et al.*, 2011a). Thus, the reconstruction of the Yangtze River caused by river system capture in the Pleistocene can be associated with stepwise Cenozoic uplift of the SE margin of the Tibetan Plateau.

Since India collided with Asia (~55 Ma), the rise of the Tibetan Plateau tandem with north-south shortening and east-west extension has affected on the surrounding regions, especially the southeast margin of the Tibetan Plateau (Tapponnier *et al.*, 2001; Zhang *et al.*, 2004). Under the influence of the east-west extension and eastward extrusion of Tibet (Schellart *et al.*, 2019), the eastward compression stress was resisted by the stable Yangtze Block on the eastern side of the Tibetan Plateau (Clark and Royden, 2000) and resulted in the formation of several large-scale sinistral strike-slip active fault zones (Wang *et al.*, 1998a, 1998b, 2000; Wang and Burchfiel, 2000; Leloup *et al.*, 2001; Tapponnier *et al.*, 2001; Burchfiel and Wang, 2003; Li *et al.*, 2022). Thus, under such a tectonic stress background, the plateau margin of NW Yunnan had achieved its present elevation (2.6–3.3 km) as early as the late Eocene (~40 Ma) as a result of the movement of rigid crustal blocks along large strike-slip faults (Hoke *et al.*, 2014; Li *et al.*, 2015; Wu *et al.*, 2018). However, the tectonic model of NE Yunnan and western Sichuan is different. Liu *et al.* (2014) identified zones of viscous crustal rocks in the deep crust that thicken eastward toward the Yangtze Block by clearly imaging the structure of the eastern Tibetan Plateau using about 300 seismographs; these were interpreted as crustal flow channels. Driven by the eastward flow of viscous rock in the deep crust since the late Miocene (beginning before ~14 Ma; Coleman and Hodges, 1995; Zhang *et al.*, 2004; Royden *et al.*, 2008; Zhang and Li, 2016), a rapid surface uplift of the western Sichuan began at ca. 13 Ma (Clark *et al.*, 2005), and NE Yunnan reached its present elevation (~1.6 km) by the same time (Li *et al.*, 2015; Wang *et al.*, 2016). Meanwhile, the farther eastern plateau margin of Guizhou had attained elevations comparable to today before the late Pliocene (Liu *et al.*, 2022b), also possibly driven by the lower crustal flow.

Based on this plateau deformation pattern, if the viscous crust rocks in the deep crust had flowed further eastward, the compression stress originating from eastward expansion of the plateau through the Sichuan Basin, which is a mechanically strong unit (Liu, 2006; Royden *et al.*, 2008; Xiang *et al.*, 2009), could have prompted deformation and surface uplift in the Huangling Dome and the Daba Mountains region, relatively weak rock between the Sichuan and Jiangnan Basins, at some time after the late Pliocene. Based on the indicator from apatite fission track data in the Huangling Dome, the uplift rate in the Huangling Dome increased from 9–13 m/Ma to 293–387 m/Ma between 7 and 0.73 Ma, and further increased from 58 m/Ma to 1033 m/Ma from 0.73 Ma to 0.01 Ma (Xiang *et al.*, 2009). Thus, the rapid increase of surface uplift of the Huangling Dome since 0.73 Ma could be the result of the lower crust flow eastward and could also be the immediate cause of the formation of the

Three Gorges and the onset of a series capture events of the paleo-Yangtze River.

Li *et al.* (2014) demonstrated that the rapid persistent rise of the Tibetan Plateau began at 8 ± 1 Ma and was followed by stepwise accelerated rises at ~3.6 Ma, 2.6 Ma, 1.8–1.7 Ma, 1.2–0.6 Ma, and 0.15 Ma based on the dating of late Cenozoic basin sediments and the tectonic geomorphology of the NE Tibetan Plateau. The cumulative effect of rise in the eastern Tibetan Plateau caused the birth of the modern Yellow River in 1.2–0.6 Ma (e.g., 0.8 Ma from Zhang *et al.* [2019]; 0.88 Ma from Yao *et al.* [2017] and Liu *et al.* [2020a]; 1.0 and 1.2 Ma from Hu *et al.* [2017 and 2019, respectively]; 1 Ma from Liu *et al.* [2019, 2022a]; 1.165 Ma from Pan *et al.* [2005b]; 1.25 Ma from Wang *et al.* [2022]). Thus, severe headward erosion, the onset of river capture events of the paleo-Yangtze River, and the formation of the Three Gorges during the period of 1.2–0.6 Ma suggest that the cumulative effect was also reflected in the evolution history of the Yangtze River. In other words, there was an intrinsic connection between the drainage evolution of the Yangtze River in SE Tibet and of the Yellow River in NE Tibet, and the evolutions of the two rivers were caused by the late Cenozoic stepwise-accelerated uplift in the eastern plateau margin (Ding *et al.*, 1995; Ren *et al.*, 2010; Li *et al.*, 2014; Zhang *et al.*, 2016) driven by the eastward expansion of the Tibetan Plateau. On the other hand, due to the effect on regional drainage evolution due to the stepwise uplift of the Tibetan Plateau, it should be reliable and effective to study the environmental effect of the Tibetan Plateau through drainage evolution.

CONCLUSIONS

The heavy mineral composition, U-Pb geochronology, and trace element composition of detrital zircons in the sediments from the Yunmeng planation surface, one river terrace, and a modern point bar in the study area have provided key information regarding the provenance changes in Quaternary fluvial deposits from Chongqing to Fengjie and the evolution of the upper Yangtze River.

First, the sediments from the Yunmeng planation surface were derived from felsic source rocks in the Huangling Dome, Wudangshan terrane, and South Qinling Belt to the east of the Three Gorges. The sediments from terrace T₅ in Chongqing primarily consist of erosional detritus from the Sichuan Basin and its peripheral areas to the west of the Three Gorges. The sediments of terrace T₂ and the modern point bar in Wanzhou consist of mafic detritus that was derived from the Shigu Group, Yidun terrane, Kangdian Rift, and Qamdo Block to the west of the Three Gorges.

Second, the provenance switch in the Quaternary fluvial deposits from Chongqing to Fengjie indicates that there was no connecting Yangtze River when the Yunmeng planation surface disintegrated at 0.75 Ma, and two rivers, the westward-flowing paleo-Chuan River and eastward-flowing paleo-Yangtze River, appeared to the west and east of the Huangling Dome, respectively. At 0.75–0.73 Ma, the paleo-Yangtze River cut through the Three Gorges and captured the paleo-Chuan River, and the Daliang Mountains became the new drainage divide between the paleo-Yangtze River and paleo-Chuan River. Finally, the paleo-Yangtze River progressively captured the paleo-Jinsha River, and a uniform large river system formed before 0.05 Ma.

Third, the reversal of flow direction of the river system of the paleo-Chuan River and formation of the modern Yangtze River

reflect the influence of the eastward expansion and stepwise-accelerated uplift of the Tibetan Plateau on the south-eastern plateau margin, which was similar on the northeastern margin.

Acknowledgments. The authors would like to thank AJE (www.aje.com) for language modification. The authors also thank Zhongyuan Chen and Hao Zou for their instructive discussions and advice.

Funding Statement. This study was supported by the Project of the National Natural Science Foundation of China (grant nos. 41972101, 41572093, 41072083).

Supplementary Material. The supplementary material for this article can be found at <https://doi.org/10.1017/qua.2022.58>

REFERENCES

- Andersen, T., 2002. Correction of common lead in U-Pb analyses that do not report ^{204}Pb . *Chemical Geology* **192**, 59–79.
- Bateman, R.M., Catt, J.A., 1985. Modification of heavy mineral assemblages in English coversands by acid pedochemical weathering. *Catena* **12**, 1–21.
- Bateman, R.M., Catt, J.A., 2007. Provenance and palaeoenvironmental interpretation of superficial deposits, with particular reference to post-depositional modification of heavy mineral assemblages. In: Mange, M.A., Wright, D.T. (Eds.), *Heavy Minerals in Use, Developments in Sedimentology*. Vol. 58. Amsterdam: Elsevier, pp. 151–188.
- Bea, F., 1996. Residence of REE, Y, Th, and U in granites and crustal protoliths; implications for the chemistry of crustal melts. *Journal of Petrology* **37**, 521–552.
- [BGMRSP] Bureau of Geology and Mineral Resources of Sichuan Provincial, 1991. *Regional Geology of Sichuan Province*. [In Chinese.] Geological Publishing House, Beijing.
- Brookfield, M., 1998. The evolution of the great river systems of southern Asia during the Cenozoic India–Asia collision: rivers draining southwards. *Geomorphology* **22**, 285–312.
- Burchfiel, B.C., Wang, E., 2003. Northwest-trending, middle Cenozoic, left-lateral faults in southern Yunnan, China, and their tectonic significance. *Journal of Structural Geology* **25**, 781–792.
- Carley, T.L., Miller, C.F., Wooden, J.L., Bindeman, I.N., Barth, A.P., 2011. Zircon from historic eruptions in Iceland: reconstructing storage and evolution of silicic magmas. *Mineralogy and Petrology* **102**, 135–161.
- Carley, T.L., Miller, C.F., Wooden, J.L., Padilla, A.J., Schmitt, A.K., Economos, R.C., Bindeman, I.N., Jordan, B.T., 2014. Iceland is not a magmatic analog for the Hadean: evidence from the zircon record. *Earth and Planetary Science Letters* **405**, 85–97.
- Cawood, P.A., Nemchin, A.A., 2000. Provenance record of a rift basin: U/Pb ages of detrital zircons from the Perth Basin, Western Australia. *Sedimentary Geology* **134**, 209–234.
- Chen, Y.L., Luo, Z.H., Zhao, J.X., Li, Z.X., Zhang, H.F., Song, B., 2004. Genesis of the Mianning–Kangding complexes from Sichuan Province: evidence from zircon SHRIMP age and geochemical features. [In Chinese.] *Science in China, Series D: Earth Sciences* **34**, 687–697.
- Clark, M.K., House, M.A., Royden, L.H., Whipple, K.X., Burchfiel, B.C., Zhang, X., Tang, W., 2005. Late Cenozoic uplift of southeastern Tibet. *Geology* **33**, 525–528.
- Clark, M.K., Royden, L.H., 2000. Topographic ooze: building the eastern margin of Tibet by lower crustal flow. *Geology* **28**, 703–716.
- Clark, M.K., Schoenbohm, L.M., Royden, L.H., Whipple, K.X., Burchfiel, B.C., Zhang, X., Tang, W., et al., 2004. Surface uplift, tectonics, and erosion of eastern Tibet from large-scale drainage patterns. *Tectonics* **23**. <https://doi.org/10.1029/2002TC001402>.
- Clift, P.D., Blusztajn, J., Nguyen, A. D., 2006. Large-scale drainage capture and surface uplift in eastern Tibet–SW China before 24 Ma inferred from sediments of the Hanoi Basin, Vietnam. *Geophysical Research Letters* **33**, L19403.
- Clift, P.D., Carter, A., Wysocka, A., Hoang, L., Zheng, H., Neubeck, N., 2020. A Late Eocene–Oligocene through-flowing river between the Upper Yangtze and South China Sea. *Geochemistry Geophysics Geosystems* **21**, e2020GC009046.
- Clift, P.D., Long, H.V., Hinton, R., Ellam, R.M., Hannigan, R., Tan, M.T., Blusztajn, J., Duc, N.A., 2008. Evolving east Asian river systems reconstructed by trace element and Pb and Nd isotope variations in modern and ancient Red River–Song Hong sediments. *Geochemistry Geophysics Geosystems* **9**, Q04039.
- Coleman, M., Hodges, K., 1995. Evidence for Tibetan plateau uplift before 14 Myr age from a new minimum age for east–west extension. *Nature* **374**, 49–52.
- Ding, L., Zhong, D.L., Pan, Y.S., Huang, X., Wang, Q.L., 1995. Fission track evidence for the Neocene rapid uplifting of the eastern Himalayan syntaxis. [In Chinese.] *Chinese Science Bulletin* **40**, 1497–1500.
- Dong, Y.P., Liu, X.M., Neubauer, F., Zhang, G.W., Tao, N., Zhang, Y.G., Zhang, X.N., Li, W., 2013. Timing of Paleozoic amalgamation between the North China and South China blocks: evidence from detrital zircon U–Pb ages. *Tectonophysics* **586**, 173–191.
- Dong, Y.P., Zhang, G.W., Hauzenberger, C., Neubauer, F., Yang, Z., Liu, X.M., 2011. Palaeozoic tectonics and evolutionary history of the Qinling orogen: evidence from geochemistry and geochronology of ophiolite and related volcanic rocks. *Lithos* **122**, 39–56.
- Dortch, J.M., Dietsch, C., Owen, L.A., Caffee, M.W., Ruppert, K., 2011a. Episodic fluvial incision of rivers and rock uplift in the Himalaya and Transhimalaya. *Journal of the Geological Society* **168**, 783–804.
- Dortch, J.M., Owen, L.A., Caffee, M.W., Kamp, D.U., 2011b. Catastrophic partial drainage of Pangong Tso, northern India and Tibet. *Geomorphology* **125**, 109–121.
- Fang, B.W., Zhang, H., Ye, R.S., Wang, Y., Chen, F.K., 2017. Petrogenesis of Laocheng granite in south Qinling: constraints from zircon U–Pb age and Sr–Nd isotopic composition. [In Chinese with English abstract.] *Journal of Earth Sciences and Environment* **39**, 633–651.
- Force, E.R., 1980. The provenance of rutile. *Journal of Sedimentary Research* **50**, 485–488.
- Fu, S., Kan, A.K., Xiao, J., Hu, J., Xiang, F., Zhang, T., Li, W.T., 2014. Research on tectonic deformation periods of structural landform landscape in the Daba Mountain National Geopark. [In Chinese with English abstract.] *Acta Geoscientia Sinica* **35**, 510–518.
- Fu, X.W., Zhu, W.L., Geng, J.H., Yang, S.Y., Zhong, K., Huang, X.T., Zhang, L.Y., Xu, X., 2021. The present-day Yangtze River was established in the late Miocene: evidence from detrital zircon ages. *Journal of Asian Earth Sciences* **205**, 104600.
- Galehouse, J.S., 1971. Point counting. In: Carver, R.E. (Ed.), *Procedures in Sedimentary Petrology*. Wiley, New York, pp. 385–407.
- Gao, W., Zhang, C.H., 2009. Zircon SHRIMP U–Pb ages of the Huangling granite and the tuff beds from Liantuo Formation in the Three Gorges area of Yangtze River, China and its geological significance. [In Chinese with English abstract.] *Geological Bulletin of China* **28**, 45–50.
- Garzanti, E., Andò, S., 2007a. Heavy mineral concentration in modern sands: implications for provenance interpretation. In: Mange, M.A., Wright, D.T. (Eds.), *Heavy Minerals in Use, Developments in Sedimentology*. Vol. 58. Elsevier, Amsterdam, pp. 517–545.
- Garzanti, E., Andò, S., 2007b. Plate tectonics and heavy mineral assemblage of modern sands. In: Mange, M.A., Wright, D.T. (Eds.), *Heavy Minerals in Use, Developments in Sedimentology*. Vol. 58. Elsevier, Amsterdam, pp. 741–763.
- Garzanti, E., Andò, S., Giovanni, V., 2009. Grain-size dependence of sediment composition and environmental bias in provenance studies. *Earth and Planetary Science Letters* **277**, 422–432.
- Gourbet, L., Leloup, P.H., Paquette, J.L., Sorrel, P., Maheo, G., Wang, G.C., Xu, Y.D., et al., 2017. Reappraisal of the Jianchuan Cenozoic basin stratigraphy and its implications on the SE Tibetan plateau evolution. *Tectonophysics* **700–701**, 162–179.
- Grimes, C.B., John, B.E., Kelemen, P.B., Mazdab, F.K., Wooden, J.L., Cheadle, M.J., Hanghøj, K., et al., 2007. Trace element chemistry of zircons from oceanic crust: a method for distinguishing detrital zircon provenance. *Geology* **35**, 643–646.
- Grimes, C.B., Wooden, J.L., Cheadle, M.J., John, B.E., 2015. “Fingerprinting” tectono-magmatic provenance using trace elements in igneous zircon. *Contributions to Mineralogy and Petrology* **170**, 1–26.

- Guan, J.L., Zheng, L.L., Liu, J.H., Sun, Z.M., Cheng, W.H., 2011. Zircons SHRIMP U-Pb dating of diabase from Hekou, Sichuan Province, China and its geological significance. [In Chinese with English abstract.] *Acta Geologica Sinica* **85**, 482–490.
- Harley, S.L., Kelly, N.M., Möller, A., 2007. Zircon behaviour and the thermal histories of mountain chains. *Elements* **3**, 25–30.
- Hartshorn, K., Hovius, N., Dade, B., Slingerland, R.L., 2002. Climate-driven bedrock incision in an active mountain belt. *Science* **297**, 2036–2038.
- He, D.F., Zhu, W.G., Zhong, H., Ren, T., Bai, Z.J., Fan, H.P., 2013. Zircon U–Pb geochronology and elemental and Sr–Nd–Hf isotopic geochemistry of the Daocheng granitic pluton from the Yidun Arc, SW China. *Journal of Asian Earth Sciences* **67–68**, 1–17.
- He, M.Y., Zheng, H.B., Bookhagen, B., Clift, P.D., 2014. Controls on erosion intensity in the Yangtze River basin tracked by U-Pb detrital zircon dating. *Earth Science Reviews* **136**, 121–140.
- Hoke, G.D., Jing, L.Z., Hren, M.T., Wissink, G.K., Garzzone, C.N., 2014. Stable isotopes reveal high southeast Tibetan Plateau margin since the Paleogene. *Earth and Planetary Science Letters* **394**, 270–278.
- Huang, H., Cawood, P.A., Hou, M.C., Yang, J.H., Ni, S.J., Du, Y.S., Zhao, K.Y., et al., 2016. Silicic ash beds bracket Emeishan Large Igneous province to <1m.y. at ~260Ma. *Lithos* **264**, 17–27.
- Hubert, J.F., 1962. A zircon–tourmaline–rutile maturity index and the interdependence of the composition of heavy minerals assemblages with the gross composition and texture of sandstones. *Journal of Sedimentary Petrology* **32**, 440–450.
- Hu, J.M., Cui, J.T., Meng, Q.R., Zhao, C.Y., 2004. The U-Pb age of zircons separated from the Zhashui granite in Qinling Orogen and its significance. [In Chinese with English abstract.] *Geological Review* **50**, 323–329.
- Hu, Z.B., Li, M.H., Dong, Z.J., Guo, L.Y., Bridgland, D., Pan, B.T., Li, X.H., Liu, X.F., 2019. Fluvial entrenchment and integration of the Sanmen Gorge, the Lower Yellow River. *Global and Planetary Change* **178**, 129–138.
- Hu, Z.B., Pan, B.T., Bridgland, D., Vandenberghe, J., Guo, L.Y., Fan, Y.L., Westaway, R., 2017. The linking of the upper–middle and lower reaches of the Yellow River as a result of fluvial entrenchment. *Quaternary Science Reviews* **166**, 324–338.
- Jia, J.T., Zheng, H.B., Huang, X.T., Wu, F.Y., Yang, S.Y., Wang, K., He, M.Y., 2010. Detrital zircon U-Pb ages of Late Cenozoic sediments from the Yangtze delta: implication for the evolution of the Yangtze River. *Chinese Science Bulletin* **55**, 1520–1528.
- Jin, G.S., 2006. *Geochronology and Geochemistry Characters on Some Magmatic Rocks in the West of Xijir Ulan-Jinshajiang Suture Zone*. [In Chinese with English abstract.] Master's thesis, Chinese Academy of Geological Sciences, Beijing (accessed November 6, 2022). https://kns.cnki.net/kcms/detail/detail.aspx?dbcode=CMFD&dbname=CMFD2008&filename=2007213514.nh&uniplatform=NZKPT&v=xSEpIRQ4I4_u5spnT4c70UZDOP-IsnGwITWNAqxoB0PKBoKnpqkxxuJ8F8qJVlfe.
- Kirkland, C.L., Smithies, R.H., Taylor, R.J.M., Evans, N., McDonald, B., 2015. Zircon Th/U ratios in magmatic enclaves. *Lithos* **212–215**, 397–414.
- Lai, S.C., Qin, J.F., 2010. *Ophiolite and Volcanic Rocks of the Mianlue Suture in the South Qinling*. [In Chinese with English abstract.] Science Press, Beijing.
- Lehnert, K., Su, Y., Langmuir, C., Sarbas, B., Nohl, U., 2000. A global geochemical database structure for rocks. *Geochemistry Geophysics Geosystems* **1**. <https://doi.org/10.1029/1999GC000026>.
- Leloup, P.H., Arnaud, N., Lacassin, R., Kienast, R.J.R., Harrison, T.M., Phan Trong, T.T., Replumaz, A., Tapponnier, P., 2001. New constraints on the structure, thermochronology, and timing of the Ailao Shan–Red River shear zone SE Asia. *Journal of Geophysical Research–Solid Earth* **106**, 6683–6732.
- Li, H.B., 2012. *Mantle Plume Geodynamic Significances of the Emeishan Large Igneous Province: Evidence from Mafic Dykes, Geochemistry and Stratigraphic Records*. [In Chinese with English abstract.] Doctoral dissertation, China University of Geoscience, Beijing (accessed November 16, 2022). <https://kns.cnki.net/kcms/detail/detail.aspx?dbcode=CDFD&dbname=CDFD1214&filename=1012364506.nh&uniplatform=NZKPT&v=pFw9nJb21RkfcZS7kzhJlcMUunkaZBR98pjw0fjPqLmob55Zd5te8dchvNhP9g0>.
- Li, H.L., Sun, Y.J., Zhang, Y.Q., 2022. Chain actions generated high-elevation and high-relief topography of the eastern margin of the Tibetan Plateau: From deep earth forces to earthquake-induced dams. *Frontiers in Earth Science* **10**, 791264.
- Li, J.J., 1991. The environmental effects of the uplift of the Qinghai–Xizang Plateau. *Quaternary Science Reviews* **10**, 479–483.
- Li, J.J., Fang, X.M., Song, C.H., Pan, B.T., Ma, Y.Z., Yan, M.D., 2014. Late Miocene–Quaternary rapid stepwise uplift of the NE Tibetan Plateau and its effects on climatic and environmental changes. *Quaternary Research* **81**, 400–423.
- Li, J.J., Xie, S.Y., Kuang, M.S., 2001. Geomorphic evolution of the Yangtze Gorges and the time of their formation. *Geomorphology* **41**, 125–135.
- Ling, W.L., Duan, R.C., Liu, X.M., Cheng, J.P., Mao, X.W., Peng, L.H., Liu, Z.X., Yang, H.M., Ren, B.F., 2010. U-Pb dating of detrital zircons from the Wudangshan Group in the South Qinling and its geological significance. *Chinese Science Bulletin* **55**, 2440–2448.
- Li, S.Y., Currie, B.S., Rowley, D.B., Ingalls, M., 2015. Cenozoic paleoaltimetry of the SE margin of the Tibetan Plateau: constraints on the tectonic evolution of the region. *Earth and Planetary Science Letters* **432**, 415–424.
- Liu, J., Chen, X.Q., Shi, W., Chen, P., Zhang, Y., Hu, J.M., Dong, S.W., Tingdong Li, T.D., 2019. Tectonically controlled evolution of the Yellow River drainage system in the Weihe region, North China: constraints from sedimentation, mineralogy and geochemistry. *Journal of Asian Earth Sciences* **179**, 350–364.
- Liu, J., Wang, P., Chen, X.Q., Shi, W., Song, L.J., Hu, J.M., 2022a. The changes in drainage systems of Weihe Basin and Sanmenxia Basin since Late Pliocene give new insights into the evolution of the Yellow River. *Frontiers in Earth Science* **9**, 820674.
- Liu, J., Zhang, J.Q., Miao, X.D., Xu, S.J., Wang, H.X., 2020a. Mineralogy of the core YRD-1101 of the Yellow River Delta: implications for sediment origin and environmental evolution during the last ~1.9Myr. *Quaternary International* **537**, 79–87.
- Liu, Q.Y., Hilst, R.D., Li, Y., Yao, H.J., Chen, J.H., Guo, B., Qi, S.H., Wang, J., Huang, H., Li, S.C., 2014. Eastward expansion of the Tibetan Plateau by crustal flow and strain partitioning across faults. *Nature Geoscience* **7**, 361–365.
- Liu, S.G., 2006. *Formation and Evolution of Dabashan Foreland Basin and Fold-and-Thrust Belt, Sichuan, China*. [In Chinese.] Geological Publishing House, Beijing.
- Liu, X.B., Chen, J., Maher, B.A., Zhao, B.C., Yue, W., Sun, Q.L., Chen, Z.Y., 2018. Connection of the proto-Yangtze River to the East China Sea traced by sediment magnetic properties. *Geomorphology* **303**, 162–171.
- Liu, X.J., Wu, R.W., Manuel, L.L., Xue, T.T., Zhou, Y., Li, K., Xu, Y., Qin, J.J., Ouyang, S., Wu, X.P., 2020b. Changes and drivers of freshwater mussel diversity patterns in the middle and lower Yangtze River Basin, China. *Global Ecology and Conservation* **22**, e00998.
- Liu, Y.S., Hu, Z.C., Zong, K.Q., Gao, C.G., Gao, S., Xu, J., Chen, H.H., 2010. Reappraisal and refinement of zircon U-Pb isotope and trace element analyses by LA-ICP-MS. *Chinese Science Bulletin* **55**, 1535–1546.
- Liu, Y.S., Hu, Z., Gao, S., Günther, D., Xu, J., Gao, C.G., Chen, H.H., 2008. In situ, analysis of major and trace elements of anhydrous minerals by LA-ICP-MS without applying an internal standard. *Chemical Geology* **257**, 34–43.
- Liu, Y., Wang, S.J., Xu, S., Fabel, D., Stuart, F.M., Rodés, Á., 2022b. New chronological constraints on the Plio-Pleistocene uplift of the Guizhou Plateau, SE margin of the Tibetan Plateau. *Quaternary Geochronology* **67**, 101237.
- Li, Y.C., Chen, J.P., Zhou, F.J., Song, S.Y., Zhang, Y.W., Gu, F.F., Cao, C., 2020. Identification of ancient river-blocking events and analysis of the mechanisms for the formation of landslide dams in the Suwalong section of the upper Jinsha River, SE Tibetan Plateau. *Geomorphology* **368**, 107351.
- Li, Y.Q., He, D.F., Li, D., Lu, R.Q., Fan, C., Sun, Y.P., Huang, H.Y., 2018. Sedimentary provenance constraints on the Jurassic to Cretaceous paleogeography of Sichuan Basin, SW China. *Gondwana Research* **60**, 15–33.
- Li, Z.X., Li, X.H., Kinny, P.D., Wang, J., Zhang, S., Zhou, H., 2003. Geochronology of Neoproterozoic syn-rift magmatism in the Yangtze Craton, South China and correlations with other continents: evidence for a mantle superplume that broke up Rodinia. *Precambrian Research* **122**, 85–109.
- Maas, R., Kinny, P.D., Williams, I.S., Froude, D.O., Compston, W., 1992. The Earth's oldest known crust: a geochronological and geochemical

- study of 3900–4200 Ma old detrital zircons from Mt. Narryer and Jack Hills, Western Australia. *Geochimica et Cosmochimica Acta* **56**, 1281–1300.
- Ma, L.F., 2002. *Atlas of Geophysics in China*. [In Chinese.] Geological Publishing House, Beijing.
- Mange, M.A., Maurer, H.F.W., 1992. *Heavy Minerals in Colour*. Chapman & Hall, London.
- Marmo, V., 1971. *Developments in Petrology 2: Granite Petrology and the Granite Problem*. Elsevier, Amsterdam.
- Ma, X.H., Li, G.H., Ying, D.L., Zhang, B.J., Li, Y., Dai, X., Fan, Y., et al., 2019. Distribution and gas-bearing properties of Permian igneous rocks in Sichuan Basin, SW China. *Petroleum Exploration and Development* **46**, 228–237.
- Ma, Y.W., Wang, G.Q., Hu, X.W., 1996. Tectonic deformation of Pengguan complex as a nappe. [In Chinese with English abstract.] *Acta Geologica Sichuan* **16**, 110–114.
- McRivette, M.W., Yin, A., Chen, X., Gehrels, G.E., 2019. Cenozoic basin evolution of the central Tibetan plateau as constrained by U–Pb detrital zircon geochronology, sandstone petrology, and fission-track thermochronology. *Tectonophysics* **751**, 150–179.
- Meng, E., Liu, F.L., Du, L.L., Liu, P.H., Liu, J.H., 2015. Petrogenesis and tectonic significance of the Baoxing granitic and mafic intrusions, southwestern China: evidence from zircon U–Pb dating and Lu–Hf isotopes, and whole-rock geochemistry. *Gondwana Research* **28**, 800–815.
- Meng, X.Y., Wang, X.X., Ke, C.H., Li, J.B., Yang, Y., Lü, X.Q., 2013. LA-ICP-MS zircon U–Pb age, geochemistry and Hf isotope of the granitoids from Huayang pluton in South Qinling orogen: Constraints on the genesis of Wulong plutons. [In Chinese with English abstract.] *Geological Bulletin of China* **32**, 1704–1719.
- Pan, B.T., Wang, J.P., Gao, H.S., Chen, Y.Y., Li, J.J., Liu, X.F., 2005a. Terrace dating as an archive of the run-through of the Sanmen Gorges. *Progress in Natural Science* **15**, 1096–1103.
- Pan, B.T., Wang, J.P., Gao, H.S., Guan, Q.Y., Wang, Y., Su, H., Li, B.Y., Li, J.J., 2005b. Paleomagnetic dating of the topmost terrace in Kouma, Henan and its indication to the Yellow River's running through Sanmen Gorges. *Chinese Science Bulletin* **50**, 657–664.
- Perrineau, A., Van Der Woerd, J., Gaudemer, Y., Jing, L.Z., Pik, R., Tapponnier, P., et al., 2011. Incision rate of the Yellow River in Northeastern Tibet constrained by ^{10}Be and ^{26}Al cosmogenic isotope dating of fluvial terraces: implications for catchment evolution and plateau building. In: Gloaguen, R., Ratschbacher, L. (Eds.), *Growth and Collapse of the Tibetan Plateau*. *Geological Society of London Special Publication* **353**, 189–219.
- Piper, D.J.W., Piper, G.P., Tubrett, M., Triantafyllidis, S., Strathdee, G., 2012. Detrital zircon geochronology and polycyclic sediment sources, Upper Jurassic–Lower Cretaceous of the Scotian Basin, southeastern Canada. *Canada Journal of Earth Sciences* **49**, 1540–1557.
- Pratt, B., Burbank, D.W., Heimsath, A., Ojha, T., 2002. Impulsive alluviation during early Holocene strengthened monsoons, central Nepal Himalaya. *Geology* **30**, 911–914.
- Qiu, Y.M., Gao, S., McNaughton, N.J., Groves, D.I., Ling, W.L., 2000. First evidence of >3.2Ga continental crust in the Yangtze craton of south China and its implications for Archean crustal evolution and Phanerozoic tectonics. *Geology* **28**, 11–14.
- Reid, A., Wilson, C.J.L., Shun, L., Pearson, N., Belousova, E., 2007. Mesozoic plutons of the Yidun arc, SW China: U–Pb geochronology and Hf isotopic signature. *Ore Geology Review* **34**, 88–106.
- Ren, Z.K., Lin, A.M., Rao, G., 2010. Late Pleistocene–Holocene activity of the Zemuhe Faults on the southeastern margin of the Tibetan Plateau. *Tectonophysics* **495**, 324–336.
- Richardson, N.J., Densmore, A.L., Seward, D., Wipf, M., Li, Y., 2010. Did incision of the Three Gorges begin in the Eocene? *Geology* **38**, 551–554.
- Roger, F., Malavieille, J., Leloup, Ph.H., Calassou, S., Xu, Z., 2004. Timing of granite emplacement and cooling in the Songpan–Garzê Fold Belt (eastern Tibetan Plateau) with tectonic implications. *Journal of Asian Earth Sciences* **22**, 465–481.
- Royden, L.H., Burchfiel, B.C., Hilst, R.D.V.D., 2008. The geological evolution of the Tibetan Plateau. *Science* **321**, 1054–1058.
- Schellart, W.P., Chen, Z., Strak, V., Duarte, J.C., Rosas, F.M., 2019. Pacific subduction control on Asian continental deformation including Tibetan extension and eastward extrusion tectonics. *Nature Communications* **10**, 4480.
- Schulz, B., Klemd, R., Braetz, H., 2006. Host rock compositional controls on zircon trace element signatures in metabasites from the Austroalpine basement. *Geochimica et Cosmochimica Acta* **70**, 697–710.
- Shellnutt, J.G., 2014. The Emeishan large igneous province: a synthesis. *Geoscience Frontiers* **5**, 369–394.
- Shen, Y.C., 1965. *Valley Geomorphology in the Upper Yangtze River*. [In Chinese.] Science Press, Beijing.
- Sircombe, K.N., 1999. Tracing provenance through the isotope ages of littoral and sedimentary detrital zircon, eastern Australia. *Sedimentary Geology* **124**, 47–67.
- Sun, X.L., Li, C.A., Kuiper, K.F., Wang, J.T., Tian, Y.T., Vermeesch, P., Zhang, Z.J., Zhao, J.X., Wijbrans, J.R., 2018. Geochronology of detrital muscovite and zircon constrains the sediment provenance changes in the Yangtze River during the late Cenozoic. *Basin Research* **30**, 636–649.
- Sun, X.L., Tian, Y.T., Kuiper, K.F., Li, C.A., Zhang, Z.J., Wijbrans, J.R., 2021. No Yangtze River prior to the Late Miocene: evidence from detrital muscovite and K-feldspar $^{40}\text{Ar}/^{39}\text{Ar}$ geochronology. *Geophysical Research Letters* **48**, e2020GL089903.
- Tang, G.Z., Tao, M., 1997. The study of the neo-tectonic movement of Changjiang Gorges region and its relation to the damage of the project construction. [In Chinese with English abstract.] *Bulletin Yichang Geology Institute* **17**, 1–70.
- Tapponnier, P., Xu, Z.Q., Roger, F., Meyer, B., Arnaud, N., Wittlinger, G., Yang, J.S., 2001. Oblique stepwise rise and growth of the Tibet Plateau. *Science* **294**, 1671–1677.
- Thompson, R.W., 1974. Mineralogy of sands from the Bengal and Nicobar fans, sites 218 and 211, Eastern Indian Ocean. In: Pimm, A.C. (Eds.), *Initial Reports of the Deep Sea Drilling Project*. Vol. 22., Texas A & M University, Ocean Drilling Program, College Station, pp. 711–713.
- Tian, L.J., Li, P.Z., Luo, Y., 1996. *Developmental History of Yangtze Gorges*. [In Chinese with English abstract.] Southwest Communications University Press, Chengdu.
- Triantafyllidis, S., Pe-Piper, G., Yang, X., Hillier, C., 2008. Detrital zircons as provenance indicators in the Lower Cretaceous sedimentary rocks of the Scotian Basin, eastern Canada: a SEM-CL study of textures. *Geological Survey of Canada Open File* 5746.
- Vermeesch, P., 2012. On the visualisation of detrital age distributions. *Chemical Geology* **312–313**, 190–194.
- Vermeesch, P., Resentini, A., Garzanti, E., 2016. An R package for statistical provenance analysis. *Sedimentary Geology* **336**, 14–25.
- Wang, B.Q., Wang, W., Chen, W.T., Gao, J.F., Zhao, X.F., Yan, D.P., Zhou, M.F., 2013a. Constraints of detrital zircon U–Pb ages and Hf isotopes on the provenance of the Triassic Yidun Group and tectonic evolution of the Yidun Terrane, eastern Tibet. *Sedimentary Geology* **289**, 74–98.
- Wang, E., Burchfiel, B.C., 2000. Late Cenozoic to Holocene deformation in southwestern Sichuan and adjacent Yunnan, China, and its role in formation of the southeastern part of the Tibetan Plateau. *Geological Society of America Bulletin* **112**, 413–423.
- Wang, E., Burchfiel, B.C., Royden, L.H., Chen, L.Z., Chen, J.S., Li, W.X., Chen, Z.L., 1998a. Late Cenozoic Xianshuihe–Xiaojiang, Red River, and Dali fault systems of southwestern Sichuan and central Yunnan, China. *Geological Society of America Special Paper* **327**, 1–108.
- Wang, H.Z., 1985. *Atlas of the Palaeogeography of China*. [In Chinese.] Cartographic Publishing House, Beijing.
- Wang, J.T., Li, C.A., Yang, Y., Wang, Q.L., 2009. The LA-ICPMS U–Pb detrital zircon geochronology and provenance study of sedimentary core in the Zhoulaotown, the Jiangnan Plain, China. [In Chinese with English abstract.] *Quaternary Sciences* **29**, 343–351.
- Wang, L.J., Yu, J.H., Griffin, W.L., O'Reilly, S.Y., 2012. Early crustal evolution in the western Yangtze Block: evidence from U–Pb and Lu–Hf isotopes on detrital zircons from sedimentary rocks. *Precambrian Research* **222–223**, 368–385.
- Wang, P., 2010. *Formation of the Western Xuefengshan Salient and the Capture and Reversal of the Middle Yangtze River, Eastern Sichuan Basin, China*. [In Chinese with English abstract.] Doctoral dissertation, China University of Geosciences, Beijing (accessed November 16, 2022). <https://doi.org/10.1017/qua.2022.58>

- kns.cnki.net/kcms/detail/detail.aspx?dbcode=CDFD&dbname=CDFD0911&filename=2010085694.
nh&uniplatform=NZKPT&v=1U7mOmkmz_Jeamh3I8fN-q7jICs2CcFtmGgUvGTKo9jMnXTG5pcN6_qkhQvcG4ri.
- Wang, P.L., Lo, C.H., Chung, S.L., Lee, T.Y., Lan, C.Y., Thang, T.V., 2000. Onset timing of left lateral movement along the Ailao Shan–Red River Shear zone: 40Ar/39Ar dating constraint from the Nam Dinh area, north-eastern Vietnam. *Journal of Asian Earth Sciences* **18**, 281–292.
- Wang, P.L., Lo, C.H., Lee, T.Y., Chung, S.L., Lan, C.Y., Yen, N.T., 1998b. Thermochronological evidence for the movement of the Ailao Shan–Red River shear zone: a perspective from Vietnam. *Geology* **26**, 887–890.
- Wang, P., Zheng, H.B., Liu, S.F., 2013b. Geomorphic constraints on middle Yangtze River reversal in eastern Sichuan Basin, China. *Journal of Asian Earth Sciences* **69**, 70–85.
- Wang, P., Zheng, H.B., Liu, S.F., 2013c. Reversal of the middle Yangtze River—tectonic geomorphic constraints in eastern Sichuan Basin. [In Chinese with English abstract.] *Quaternary Sciences* **33**, 631–644.
- Wang, X., Hu, G., Saito, Y., Ni, G.Z., Hu, H., Yu, Z.Y., Chen, J.P., *et al.*, 2022. Did the modern Yellow River form at the mid-Pleistocene transition? *Science Bulletin* **67**, 1603–1610.
- Wang, Y.Y., Fan, D.D., 2013. U–Pb ages and Hf isotopic composition of crystalline zircons from igneous rocks of the Changjiang drainage basin and their implications for provenance. [In Chinese with English abstract.] *Marine Geology & Quaternary Geology* **33**, 97–118.
- Wang, Y., Zhang, B., Schoenbohm, L.M., Zhang, J.J., Zhou, R.J., Hou, J.J., Ai, S., 2016. Late Cenozoic tectonic evolution of the Ailao Shan–Red River fault (SE Tibet): implications for kinematic change during plateau growth. *Tectonics* **35**, 1969–1988.
- Wei, J.Q., Wang, J.X., 2012. Zircon age and Hf isotope compositions of amphibolite enclaves from the Kongling Complex. [In Chinese with English abstract.] *Geological Journal of China Universities* **18**, 589–600.
- Wei, J.Q., Wang, J.X., Wang, X.D., Shan, M.Y., Guo, H.M., 2009. Dating of mafic dikes from Kongling Group in Huangling Area and its implications. [In Chinese with English abstract.] *Journal of Northwest University (Natural Science Edition)* **39**, 466–471.
- Wei, J.Q., Wei, Y.X., Wang, J.X., Wang, X.D., 2020. Geochronological constraints on the formation and evolution of the Huangling basement in the Yangtze craton, South China. *Precambrian Research* **345**, 1–12.
- Weislogel, A.L., 2008. Tectonostratigraphic and geochronologic constraints on evolution of the northeast Paleotethys from the Songpan–Ganzi complex, central China. *Tectonophysics* **451**, 331–345.
- Wu, C., Ji, S.C., Cao, H., Dong, H.W., Chen, X.J., 2021. Jurassic post-collisional extension in the Songpan–Ganze Terrane, eastern Tibetan Plateau: evidence from weakly peraluminous A-type granites within the Zheduo–Gongga Massif. *Geological Journal* **56**, 1911–1931.
- Wu, J., Zhang, K.X., Xu, Y.D., Wang, G.C., Garzzone, C.N., Eiler, J., Leloup, P.H., Sorrel, P., Mahéo, G., 2018. Paleoelevations in the Jianchuan Basin of the southeastern Tibetan Plateau based on stable isotope and pollen grain analyses. *Palaeogeography, Palaeoclimatology, Palaeoecology* **510**, 93–108.
- Xiang, F., 2004. *Forming of the Three Gorges of the Yangtze River and Sedimentary Response in the West Edge of Jiangnan Basin and Adjacent Area*. [In Chinese with English abstract.] Doctoral dissertation, Chengdu University of Technology, Chengdu (accessed November 16, 2022). <https://kns.cnki.net/kcms/detail/detail.aspx?dbcode=CDFD&dbname=CDFD9908&filename=2004085871.nh&uniplatform=NZKPT&v=9o07eFhhVOPiY20gweEduQ4e3JBVYc9tV6ZGwUiyk18vyMk6x2NZteQS3mCwz0y>.
- Xiang, F., Du, W., Huang, H.X., Kang, D.Y., Zhu, H.B., Feng, Q., 2018. Provenance study of Fe–Ti oxide minerals in the Quaternary sediments in Yichang area and its implication of formation time of the Yangtze Three Gorges, China. *Acta Geologica Sinica (English Edition)* **92**, 1598–1608.
- Xiang, F., Huang, H.X., Ogg, J.G., Zhu, H.B., Kang, D.Y., 2020. Quaternary sediment characteristics and paleoclimate implications of deposits in the Three Gorges and Yichang areas of the Yangtze River. *Geomorphology* **351**, 106981.
- Xiang, F., Li, Z.H., Wang, C.S., Zhu, L.D., Liu, S., 2009. Cenozoic uplift characteristics of Shandouping section of Huangling Dome in the west of Hubei Province. [In Chinese with English abstract.] *Acta Geologica Sinica* **83**, 1247–1254.
- Xiang, F., Yang, D., Tian, X., Li, Z.H., Lu, L., 2011. LA-ICP-MS U–Pb geochronology of zircons in the Quaternary sediments from the Yichang area of Hubei Province and its provenance significance. [In Chinese with English abstract.] *Journal of Mineralogy and Petrology* **31**, 106–114.
- Xiang, F., Zhu, L.D., Wang, C.S., Li, Y.Z., Yang, W.G., 2005. Terrace age correlation and its significance in research of Yangtze Three Gorges, China. [In Chinese with English abstract.] *Journal of Chengdu University of Technology (Science Technology Edition)* **32**, 162–166.
- Yang, C.Q., Shen, C.B., Massimiliano, Z., Yu, W., Shi, S.X., Mei, L.F., 2019. Provenances of Cenozoic sediments in the Jiangnan Basin and implications for the formation of the Three Gorges. *International Geology Review* **61**, 1980–1999.
- Yang, J.K., 2014. *Geochemical Characteristics of Metamorphic Rock Series in the Upper Member of Shigu Group in Badi Area, Northwest Yunnan*. [In Chinese with English abstract.] Master's thesis, Kunming University of Science and Technology, Kunming (accessed November 16, 2022). <https://kns.cnki.net/kcms/detail/detail.aspx?dbcode=CDFD&dbname=CDFD201501&filename=1014356284.nh&uniplatform=NZKPT&v=3pn6eV2GqoM-JN3V4jMJEZC4xRC3WGbchnFNj6wNiKcmgiSR9HN100Fp2RQ3bH>.
- Yang, K., Liu, S.W., Li, Q.G., Wang, Z.Q., Han, Y.G., Wu, F.H., Zhang, F., 2009. LA-ICP-MS zircon U–Pb geochronology and geological significance of Zhushui granitoids and Dongjiangkou granitoids from Qinling, central China. [In Chinese with English abstract.] *Acta Scientiarum Naturalium Universitatis Pekinensis* **45**, 841–847.
- Yang, S.Y., Li, C.X., Yokoyama, K., 2006. Elemental compositions and monazite age patterns of core sediments in the Changjiang Delta: implications for sediment provenance and development history of the Changjiang River. *Earth and Planetary Science Letters* **245**, 762–776.
- Yan, Q.R., Hanson, A.D., Wang, Z.Q., Druschke, P.A., Yan, Z., Wang, T., Liu, D.Y., *et al.*, 2004. Neoproterozoic subduction and rifting on the northern margin of the Yangtze plate, China: implications for Rodinia reconstruction. *International Geology Review* **46**, 817–832.
- Yan, Q.R., Wang, Z.Q., Hanson, A.D., Druschke, P.A., Yan, Z., Liu, D.Y., Jian, P., *et al.*, 2003. SHRIMP age and geochemistry of the Bikou volcanic terrane: implications for Neoproterozoic tectonics on the northern margin of the Yangtze Craton. [In Chinese with English abstract.] *Acta Geologica Sinica* **77**, 479–490.
- Yao, Z.Q., Shi, X.F., Qiao, S.Q., Liu, Q.S., Kandasamy, S., Liu, J.X., Liu, Y.G., *et al.*, 2017. Persistent effects of the Yellow River on the Chinese marginal seas began at least ~880 ka ago. *Scientific Reports* **7**, 2827.
- Yuan, C., Zhou, M.F., Sun, M., Zhao, Y.J., Wilde, S., Long, X.P., Yan, D.P., 2010. Triassic granitoids in the eastern Songpan Ganzi Fold Belt, SW China: magmatic response to geodynamics of the deep lithosphere. *Earth and Planetary Science Letters* **290**, 481–492.
- Zhang, G.W., Guo, A.L., Wang, Y.J., Li, S.Z., Dong, Y.P., Liu, S.F., He, D.F., *et al.*, 2013. Tectonics of South China continent and its implications. *Science China Earth Sciences* **56**, 1804–1828.
- Zhang, J., Wan, S.M., Clift, P.D., Huang, J., Yu, Z.J., Zhang, K.D., Mei, X., *et al.*, 2019. History of Yellow River and Yangtze River delivering sediment to the Yellow Sea since 3.5 Ma: tectonic or climate forcing? *Quaternary Science Reviews* **216**, 74–88.
- Zhang, P.Z., Shen, Z.K., Wang, M., Gan, W.J., Burgmann, R., Molnar, P., *et al.*, 2004. Continuous deformation of the Tibetan Plateau from global positioning system data. *Geology* **32**, 809–812.
- Zhang, S.B., Zheng, Y.F., Zhao, Z.F., Wu, Y.B., Yuan, H.L., Wu, F.Y., 2009. Origin of TTG-like rocks from anatexis of ancient lower crust: geochemical evidence from Neoproterozoic granitoids in South China. *Lithos* **113**, 347–368.
- Zhang, X.B., Liu, Y., Wang, S.J., Liu, W.M., Xue, W.X., 2018. On the chronology of the Yellow Rivers and the Yangtze Rivers. [In Chinese with English abstract.] *Mountain Research* **36**, 661–668.
- Zhang, Y.N., Li, R.X., Liu, H.Q., Zhu, R.J., Zhu, D.M., Wang, N., Zhao, B.S., 2014. Mesozoic–Cenozoic tectonic uplift history of Dabashan foreland structure in the northern rim of Sichuan Basin. [In Chinese with English abstract.] *Journal of Earth Sciences and Environment* **36**, 230–238.
- Zhang, Y.Q., Li, H.L., 2016. Late Cenozoic tectonic events in east Tibetan Plateau and extrusion-related orogenic system. [In Chinese with English abstract.] *Geology in China* **43**, 1829–1852.
- Zhang, Y.Q., Li, H.L., Li, J., 2016. Neotectonics of the eastern margin of the Tibetan Plateau: new geological evidence for the change from Early

- Pleistocene transpression to Late Pleistocene–Holocene strike-slip faulting. *Acta Geologica Sinica (English Edition)* **90**, 467–485.
- Zhang, Z.J.**, 2020. Analysis on the characteristics and genesis of Kangding complex. [In Chinese.] *Western Resources*, 37–39.
- Zhang, Z.J., Stephen Daly, J., Li, C.A., Tyrrell, S., Sun, X.L., Badenszki, E., Li, Y.W., Zhang, D., Tian, Y.T., Yan, Y.**, 2021. Formation of the Three Gorges (Yangtze River) no earlier than 10 Ma. *Earth Science Reviews* **216**, 103601.
- Zhang, Z.Q., Zhang, G.W., Tang, S.H.**, 2002. *Isotopic Geochronology of Metamorphic Strata in South Qinling Mountains*. [In Chinese.] Geological Publishing House, Beijing, pp. 231–246.
- Zhao, F.Q., Zhao, W.P., Zuo, Y.C., Li, Z.H.**, 2006a. Zircon U-Pb ages of the migmatites from Kongling Complex. [In Chinese with English abstract.] *Geology Survey and Research* **29**, 3–7.
- Zhao, F.Q., Zhao, W.P., Zuo, Y.C., Li, Z.H. Xue, K.Q.**, 2006b. U-Pb geochronology of Neoproterozoic magmatic rocks in Hanzhong, southern Shaanxi, China. [In Chinese with English abstract.] *Geology Bulletin of China* **25**, 383–388.
- Zhao, J.H., Zhou, M.F.**, 2008. Neoproterozoic adakitic plutons in the northern margin of the Yangtze Block, China: partial melting of a thickened lower crust and implications for secular crustal evolution. *Lithos* **104**, 231–248.
- Zhao, J.H., Zhou, M.F.**, 2009. Secular evolution of the Neoproterozoic lithospheric mantle underneath the northern margin of the Yangtze Block, South China. *Lithos* **107**, 152–168.
- Zhao, M., Wei, J.Q., Wang, J.X.**, 2012. Zircon U-Pb Age and Hf isotope composition from Yemadong mafic dikes in the Huangling area. [In Chinese with English abstract.] *Geology and Mineral Resources of South China* **28**, 124–131.
- Zheng, H.B.**, 2015. Birth of the Yangtze River: age and tectonic-geomorphic implications. *National Science Review* **2**, 438–453.
- Zheng, H.B., Clift, P.C., Wang, P., Tada, R.J., Jia, J.T., He, M.Y., Jourdan, F.**, 2013. Pre-Miocene birth to the Yangtze River. *Proceedings of the National Academy of Sciences USA* **110**, 7556–7561.
- Zhong, L.M., Xu, M., Yang, Y.N., Wang, X.B.**, 2018. The development and evolution of landform based on neotectonic movement: The Sancha river catchment in the southwestern China. *Journal of Earth System Science* **127**, article 8.
- Zhou, D., Graham, S.A.**, 1996. Extrusion of the Altyn Tagh wedge: a kinematic model for the Altyn Tagh fault and palinspastic reconstruction of northern China. *Geology* **24**, 427–430.
- Zhou, M.F., Yan, D.P., Kennedy, A.K., Li, Y.Q., Ding, J.**, 2002. SHRIMP U-Pb zircon geochronological and geochemical evidence for Neoproterozoic arc-magmatism along the western margin of the Yangtze Block, South China. *Earth and Planetary Science Letters* **196**, 51–67.
- Zhou, M.F., Yan, D.P., Wang, C.L., Qi, L., Kennedy, A.**, 2006. Subduction-related origin of the 750Ma Xuelongbao adakitic complex (Sichuan Province, China): implications for the tectonic setting of the giant Neoproterozoic magmatic event in South China. *Earth and Planetary Science Letters* **248**, 286–300.
- Zou, H., Bagas, L., Li, X.Y., Liu, H., Jiang, X.W., Li, Y.**, 2020. Origin and evolution of the Neoproterozoic Dengganping granitic complex in the western margin of the Yangtze Block, SW China: implications for breakup of Rodinia supercontinent. *Lithos* **370–371**, 105602.
- Zou, H., Li, Q.L., Bagas, L., Wang, X.C., Chen, A.Q., Li, X.H.**, 2021. A Neoproterozoic low- $\delta^{18}\text{O}$ magmatic ring around South China: implications for configuration and breakup of Rodinia supercontinent. *Earth and Planetary Science Letters* **575**, 117196.